Published in final edited form as:
Nat Metab. 2020 February ; 2(2): 142–152. doi:10.1038/s42255-020-0173-1.

T1D progression is associated with loss of CD3$^+$CD56$^+$ regulatory T cells that control CD8$^+$ T cell effector functions

Giuseppe Terrazzano[#1,2], **Sara Bruzzaniti**[#3,4], **Valentina Rubino**[#1,2], **Marianna Santopaolo**[3], **Anna Teresa Palatucci**[1], **Angela Giovazzino**[2], **Claudia La Rocca**[3], **Paola de Candia**[5], **Annibale Puca**[5], **Francesco Perna**[6], **Claudio Procaccini**[3,7], **Veronica De Rosa**[3,7], **Chiara Porcellini**[2], **Salvatore De Simone**[3], **Valentina Fattorusso**[2], **Antonio Porcellini**[4], **Enza Mozzillo**[2], **Riccardo Troncone**[2,8], **Adriana Franzese**[2], **Johnny Ludvigsson**[9], **Giuseppe Matarese**[3,10,*], **Giuseppina Ruggiero**[2,*], **Mario Galgani**[3,10,*]

[1]Dipartimento di Scienze, Università degli Studi di Potenza, Potenza 85100, Italy

[2]Dipartimento di Scienze Mediche Traslazionali, Università degli Studi di Napoli "Federico II", Naples 80131, Italy

[3]Laboratorio di Immunologia, Istituto per l'Endocrinologia e l'Oncologia Sperimentale "G. Salvatore", Consiglio Nazionale delle Ricerche, Naples 80131, Italy

[4]Dipartimento di Biologia, Università degli Studi di Napoli "Federico II", Naples 80126, Italy

[5]Istituto di Ricovero e Cura a Carattere Scientifico MultiMedica, Milan 20138, Italy

[6]Dipartimento di Medicina Clinica e Chirurgia, Università degli Studi di Napoli "Federico II", Naples 80131, Italy

[7]Unità di Neuroimmunologia, Fondazione Santa Lucia, Rome 00143, Italy

[8]European Laboratory for the Investigation of Food-Induced Disease (ELFID), Università degli Studi di Napoli "Federico II", Naples 80131, Italy

[9]Div of Pediatrics, Dept of Biomedical and clinical sciences, Linköping University, and Crown Princess Victoria Children's Hospital, Region Östergötland, Linköping, Sweden

[*]Correspondence should be addressed to M.G. (mario.galgani@unina.it), G.R. (giruggie@unina.it) or G.M. (giuseppe.matarese@unina.it).

Data availability

The data that support the findings of this study are available from the corresponding authors upon request. Transcriptional data of $T_{R3\text{-}56}$, NK, CD3$^+$CD56$^-$, CD8$^+$ cells from adult healthy subjects are in the GEO database with accession code GSE106082. Transcriptional data of $T_{R3\text{-}56}$ cells from T1D and healthy children are in the GEO database with accession code GSE134916.

Authors Contributions

S.B., V.R. and M.S. performed most of the experiments and data analyses; A.T.P., A.G., C.L.R. and S.D.S. performed the experiments and data analyses; F.P. and S.B. performed flow cytometry experiments and data analyses; S.B., V.R., M.S., G.T., G.R., A.Po., V.D.R. and C.Pr. and M.G. analysed the data and interpreted the results; A.Pu. and P.d.C. analysed transcriptional data; V.D.R., A.Po. and C.Pr. were involved in the discussion about the data; J.L., C.Po., V.F., E.M., R.T. and A.F. provided human samples from the patients and were involved in discussion about the data; P.d.C., G.T., G.R., J.L., G.M. and M.G. designed the study and wrote the manuscript.

Competing Financial Interests

The authors declare no competing financial interests.

Reporting Summary

Further information on research design is available in the Nature Research Reporting Summary linked to this article.

Europe PMC Funders Author Manuscripts

[10]Dipartimento di Medicina Molecolare e Biotecnologie Mediche, Università degli Studi di Napoli "Federico II", Naples 80131, Italy

[#] These authors contributed equally to this work.

Abstract

An unresolved issue in autoimmunity is the lack of surrogate biomarkers of immunological self-tolerance for disease monitoring. Here, we show that peripheral frequency of a regulatory T cell population, characterized by the co-expression of CD3 and CD56 molecules ($T_{R3\text{-}56}$), is reduced in subjects with new-onset type 1 diabetes (T1D). In three independent T1D cohorts, we find that low frequency of circulating $T_{R3\text{-}56}$ cells is associated with reduced β-cell function and with the presence of diabetic ketoacidosis. As autoreactive $CD8^+$ T cells mediate disruption of insulin-producing β-cells[1–3], we demonstrate that $T_{R3\text{-}56}$ cells can suppress $CD8^+$ T cell functions *in vitro* by reducing levels of intracellular reactive oxygen species. The suppressive function, phenotype and transcriptional signature of $T_{R3\text{-}56}$ cells are also altered in T1D children. Together, our findings indicate that $T_{R3\text{-}56}$ cells constitute a regulatory cell population that controls $CD8^+$ effector functions, whose peripheral frequency may represent a traceable biomarker for monitoring immunological self-tolerance in T1D.

T1D is an autoimmune disease characterized by T cell-mediated destruction of insulin producing β-cells in the pancreas[2]. An unresolved issue in T1D is the lack of biomarkers able to track immunological self-tolerance and disease progression in autoimmune disorders such as T1D. Peripheral blood of healthy individuals contains a T cell subset co-expressing CD3 and CD56 molecules[4], whose peripheral frequency has been associated with different pathological conditions[5,6]. We recently observed that the number of $CD3^+CD56^+$ T cells present at T1D diagnosis, directly reflected residual β-cell function one-year later[7].

To gain further insight into the physio-pathological relevance and the potential regulatory function of $CD3^+CD56^+$ T cells (herein defined as $T_{R3\text{-}56}$ cells), we first enumerated circulating $T_{R3\text{-}56}$ cells (see Supplementary Figure 1 for gating strategy) in a large cohort (enrolled in Campania Region of Italy, herein "Italian cohort") of pre-puberty T1D children at disease onset (n=128), in comparison with healthy children (n=113) (Supplementary Table 1). We found that T1D children had reduced percentage and absolute number of $T_{R3\text{-}56}$ cells compared with healthy controls (Fig. 1a, **left** and **right**). The observed differences were maintained also after adjusting the comparison for sex, age and body mass index (BMI) (Extended Data 1a, **left** and **right**). The lower frequency of circulating $T_{R3\text{-}56}$ cells in T1D subjects associated, at least in part, with their increased rate of necrotic death (1.5% ± 0.14, 3.9% ± 0.44 for healthy and T1D subjects, respectively), while no difference was observed in apoptosis (Extended Data 1b, **left** and **right**).

Next, we asked whether $T_{R3\text{-}56}$ cells associated with residual pancreatic β-cell function (measured as circulating fasting C-peptide) in T1D at disease onset. To this end we performed a bivariate analysis that revealed a positive correlation between peripheral frequency and absolute number of $T_{R3\text{-}56}$ cells and fasting C-peptide levels ($r=0.71$, $p<0.0001$; $r=0.57$, $p<0.0001$, respectively) (Fig. 1b,c).

As diabetic ketoacidosis (DKA), haemoglobin A1c (HbA1c) and daily insulin dose strongly influence T1D complication overtime[8,9], we applied a logistic regression modeling on these parameters and revealed that low percentages of $T_{R3\text{-}56}$ cells were able to predict DKA at disease onset (Extended Data 1c, **left**). Prognostic validity of the fitted model was evaluated by receiver operating characteristic (ROC) curve analysis and measured using the area under the curve (AUC) (Extended Data 1c, right). Low absolute counts of $T_{R3\text{-}56}$ cells also associated with the presence of DKA (Extended Data 1d, **left** and **right**). Finally, the frequency and absolute numbers of $T_{R3\text{-}56}$ cells did not associate either with HbA1c values or with daily insulin dose (Supplementary Figure 2).

We corroborated our findings also in post-puberty young T1D adults at diagnosis (Italian cohort, n=19) (Supplementary Table 2). Specifically, we observed that $T_{R3\text{-}56}$ cell frequency and absolute number were reduced compared to age-matched healthy subjects (n=14) (Fig. 1d, **left** and **right**), positively correlated with plasma levels of fasting C-peptide (r=0.46, p=0.047; r=0.50, p=0.0369, respectively) (Fig. 1e,f) and negatively associated with presence of DKA (Extended Data 1e,f).

Then, to further validate $T_{R3\text{-}56}$ cells as traceable biomarker of T1D progression, we analysed an independent cohort of children with recent-onset T1D (n=36) recruited at Linköping University Hospital, Sweden (Supplementary Table 3). In this validation cohort (herein defined as “Swedish cohort”), bivariate analysis further confirmed that the frequency of circulating $T_{R3\text{-}56}$ cells positively correlated with fasting C-peptide (r=0.63, p<0.0001) (Fig. 2a).

Next, we measured specificity of our findings in a third independent cohort of T1D subjects (n=44) recruited at European Laboratory for the Investigation of Food-Induced Disease (ELFID), University of Napoli “Federico II” (Supplementary Table 4), in which T1D at diagnosis was associated or not with another autoimmune disorder/immune dysregulation [(either autoimmune thyroiditis (AIT) or coeliac disease (CD)]. Strikingly, in 23 out of 44 children at T1D diagnosis (going to develop also CD or AIT in the following three years), bivariate analysis confirmed the positive correlation between $T_{R3\text{-}56}$ cells and fasting C-peptide levels (r=0.57, p=0.0043) (Fig. 2b). Logistic regression modeling established that peripheral percentages of $T_{R3\text{-}56}$ cells indicated the presence of DKA (Extended Data 2a **left** and **right**). On the contrary, in 21 out of the 44 children that at T1D diagnosis were already affected by either CD or AIT, $T_{R3\text{-}56}$ cells did not show statistical correlation with fasting C-peptide levels (r=-0.003, p=0.9901) (Fig. 2c), and weakly associated with the presence of DKA (Extended Data 2b, **left** and **right**).

To exclude that the association between $T_{R3\text{-}56}$ cells and C-peptide relied on metabolic alterations (i.e. hyperglycaemia and DKA) both typical of T1D onset, we assessed their frequency also in T1D subjects (n=31) one year after T1D diagnosis when metabolic alterations have been stabilized. In these subjects, we found that $T_{R3\text{-}56}$ cell frequency positively correlated with plasma levels of fasting C-peptide (r=0.53, p=0.0023) and reflected residual β-cell mass (Fig. 2d).

Finally, to rule out the possibility of a bias induced by the presence of possible outliers in the peripheral frequency of $T_{R3\text{-}56}$ cells, analyses excluding these subjects were performed and also revealed statistical correlation between $T_{R3\text{-}56}$ cells and fasting C-peptide (Supplementary Figure 2).

To investigate whether frequency of $T_{R3\text{-}56}$ cells also associated with pre-symptomatic stages of T1D, we measured the frequency of $T_{R3\text{-}56}$ cells in 51 at-risk subjects, siblings of T1D individuals from our main "Italian cohort" followed over time every six months from 2015. This included 35 autoantibody negative (Ab), 9 autoantibody positive (Ab^+) and 7 autoantibody positive that reverted into autoantibody negative (Ab reverted) subjects. Interestingly, we observed that frequency of $T_{R3\text{-}56}$ cells was significantly higher in "Ab reverted" subjects compared with healthy, Ab^- and Ab^+ children (Fig. 2e). We also noticed a significant reduction of $T_{R3\text{-}56}$ cells in Ab^+ subjects with respect to healthy individuals (Fig. 2e). In all, peripheral frequency of $T_{R3\text{-}56}$ cells can act as specific non-invasive T1D biomarker able to reflect disease progression and severity in T1D at onset and far from diagnosis. However, further investigations on larger cohorts of at-risk subjects are need to confirm $T_{R3\text{-}56}$ cells as biomarker of early asymptomatic phase of disease.

Moreover, if the development of T1D was anticipated by another immune-mediated disorder (either CD or AIT), $T_{R3\text{-}56}$ cells failed to predict T1D progression, probably as consequence of confounding factors related to an already compromised immunological self-tolerance associated with the first autoimmune disorder.

Since high frequency of $T_{R3\text{-}56}$ cells associated with a preserved residual β-cell reservoir, we hypothesised a possible, unexplored, immune regulatory role for this cellular subset. To test this hypothesis, first we characterized $T_{R3\text{-}56}$ cells in adult healthy donors and subsequently we assessed their function, surface phenotype and molecular profile in T1D children. Specifically, we measured the capacity of flow-sorted human $T_{R3\text{-}56}$ cells to affect proliferation of *in vitro* T cell receptor (TCR)-stimulated human $CD8^+$ and $CD4^+$ T cells from adult healthy donors. Strikingly, we observed that $T_{R3\text{-}56}$ cells inhibited proliferation of both $CD8^+$ and $CD4^+$ T cells (Fig. 3a), with the main suppressive effect on the proliferation of the $CD8^+$ subset (Fig. 3a). These findings prompted us to focus on the ability of $T_{R3\text{-}56}$ cells to suppress effector/cytotoxic functions of $CD8^+$ T lymphocytes. We evaluated the ability of $T_{R3\text{-}56}$ cells to control cytotoxicity of human $CD8^+$ T cells (effectors) against allogeneic target (see experimental procedure Supplementary Figure 3). Specifically, $T_{R3\text{-}56}$ cells, compared with control cells, suppressed lytic capacity of $CD8^+$ effector cells at different effector:target *ratio* (Fig. 3b). Next, we further explore the regulatory activity of $T_{R3\text{-}56}$ cells on cytolytic T lymphocytes (CTLs), generated from $CD8^+$ T cells stimulated with human recombinant (hr) IL-2 in vitro[10,11] (see experimental procedure Supplementary Figure 4). CTLs were co-cultured with $T_{R3\text{-}56}$ cells or control cells and stimulated for 4 hours *via* TCR to evaluate cytotoxic activity (measured by CD107a/LAMP-1 expression as readout of cytotoxicity[12,13]) and IFN-γ production by CTLs (see experimental procedure Supplementary Figure 4 and gating strategy Supplementary Figure 5). $T_{R3\text{-}56}$ cells significantly suppressed CTL effector functions, while addition of either Natural Killer (NK) or $CD8^+$ T cells (as internal control), was unable to affect CD107a/LAMP-1 expression and

IFN-γ production by CTLs (Fig. 3c). We found that $T_{R3\text{-}56}$ cell suppressive functions were maintained also in co-culture with allogeneic CTLs (Extended Data 4a).

To identify the molecular mechanisms of $T_{R3\text{-}56}$ cell suppression, we assessed whether this function relied on either cell-to-cell contact, secretion of soluble factors or both. Trans-well experiments revealed that $T_{R3\text{-}56}$ cells were unable to exert regulatory activity when separated from CTLs (Fig. 3d and Extended Data 4b). Therefore, their contact-mediated suppressive activity was independent on the expression of CD56 molecules (Extended Data 4c).

ROS-mediated signalling has been frequently associated with degranulation processes and IFN-γ production by CTLs[14,15]. We studied dynamic changes of cytosolic and mitochondrial ROS levels upon TCR-stimulation of CTLs cultured with $T_{R3\text{-}56}$ cells. Cytosolic CTLs ROS levels, evaluated by 2',7'-dichlorodihydrofluorescein diacetate (DCF) staining, were significantly reduced by $T_{R3\text{-}56}$ cells (Fig. 3e); control cells (NK or $CD8^+$ T cells) did not influence cellular ROS levels in CTLs (Fig. 3e). Conversely, $T_{R3\text{-}56}$ cells did not affect mitochondrial-derived ROS in CTLs, as testified by mitoSOX staining (Supplementary Figure 6). To confirm the role of cellular ROS in mediating $T_{R3\text{-}56}$ cell regulatory activity, we took advantage of the ability of menadione, an analogue of 1,4-naphthoquinone, to generate intracellular ROS *via* redox cycling[16,17]. $T_{R3\text{-}56}$ cells are unable to suppress CD107a/LAMP-1 expression and IFN-γ of menadione pre-treated CTLs (Fig. 3f and Extended Data 5). In addition, menadione *per se* was unable to induce *in vitro* CTL activation in absence of TCR stimulation (Extended Data 5). To note, treatment with the ROS-inhibitor, N-acetyl-L-cysteine (NAC), completely blocked CTL activation[18], suggesting that $T_{R3\text{-}56}$ cells control $CD8^+$ responses by modulating cytosolic ROS.

Finally, adult $T_{R3\text{-}56}$ cells were also characterized for metabolic features (glycolysis and oxidative phosphorylation) and their transcriptional signature. Seahorse analysis revealed that upon TCR stimulation, $T_{R3\text{-}56}$ cells have a distinct metabolic phenotype compared to NK, $CD8^+$ and $CD4^+$ cells, as preferentially utilizing OXPHOS as the main cellular bio-energetic source (Supplementary Figure 7). Microarray analysis of RNA from $T_{R3\text{-}56}$ cells revealed their distinct transcriptomic signature, compared to NK, $CD3^+CD56^-$ and $CD8^+$ subsets (Supplementary Figure 8).

Compelling experimental evidence supports the central role of T lymphocytes in immune-mediated damage of β-cells in T1D[19–21]. Autoreactive $CD8^+$ T lymphocytes kill β-cells through release of cytolytic granules and by production of tissue damaging pro-inflammatory cytokines[22,23]. As specific regulatory networks targeting $CD8^+$ T cell functions are still poorly understood in T1D, we explored whether human $T_{R3\text{-}56}$ cells are involved in T1D pathogenesis. We evaluated suppressive capability, phenotype, cytokine production and transcriptomic-molecular signature of $T_{R3\text{-}56}$ cells isolated from recent-onset T1D subjects in comparison with those of healthy children. Notably, $T_{R3\text{-}56}$ cells isolated from newly diagnosed T1D subjects had a decreased ability to modulate TCR-dependent CD107a/LAMP-1 expression of autologous CTLs (Fig. 4a). This impaired suppressive function was not due to the presence of suppression-resistant $CD8^+$ T cells in T1D subjects, since CTLs from T1D resulted to be sensitive to regulatory activity of $T_{R3\text{-}56}$ cells from

healthy individuals (Fig. 4b). These results indicate that suppressive capability of $T_{R3\text{-}56}$ cells is impaired in T1D children at diagnosis.

Surface phenotypic analysis revealed that $T_{R3\text{-}56}$ cells from recent-onset T1D children were comparable to healthy controls for CD4, CD8, CD45RA, CD45RO and CD27 expression while CD28 surface levels were significantly higher in $T_{R3\text{-}56}$ cells from T1D subjects (Fig. 4c and Extended Data 6a, **left** and **right**). Also, $T_{R3\text{-}56}$ cells from T1D children had reduced surface expression of activating/inhibitor receptors (CD94, NKG2A, NKG2C, NKG2D, DNAM-1 and CD16)[24] and cytotoxicity-related molecule (Granzyme-B)[23], compared to healthy children (Fig. 4c). On the other hand, $T_{R3\text{-}56}$ cells from recent-onset T1D children expressed increased surface levels of chemokine receptors homing cells in the pancreas, such as CXCR3, CXCR4 and CCR7 (Fig. 4c)[25–27]. Low or moderate levels of main T_{Reg} cell-associated markers[28], such as CD25, the transcription factor forkhead box P3 (FoxP3), CTLA-4, CD39, GITR and PD-1 were expressed on $T_{R3\text{-}56}$ cells from both control and T1D subjects (Supplementary Figure 9).

Finally, FACS analysis revealed that $T_{R3\text{-}56}$ cells from both healthy controls and T1D subjects are distinct from the invariant (i)NKT subset[29,30], as they are not CD1d-restricted**,** do not express Vα24/Vβ11 TCR chains and display a heterogeneous β TCR repertoire (**Extended Data 6a,b**).

Multiplex cytokine analysis showed that $T_{R3\text{-}56}$ cells from new onset T1D individuals released, upon 48 hours of TCR stimulation, reduced amount of IFN-γ, IL-2, IL-4, IL-13, IL-21, IL-22, TNF-α compared with healthy children (Fig. 4d); on the other side, $T_{R3\text{-}56}$ cells from T1D children secreted increased amounts of IL-15 and IL-17A (Fig. 4d), while no significant differences were observed for other cytokines such as IL-8, IL-9, IL-10, IL-31, TNF-β (Fig. 4d). Furthermore, an un-biased high-throughput analysis (RNA-seq) of the transcriptome expressed by $T_{R3\text{-}56}$ cells from T1D children in comparison with age- and sex-matched healthy controls revealed the dysregulation of several genes that may contribute to T1D-depedent functional impairment of this cell subset. In particular, we concentrated our attention on genes (n=33, see Fig. 4e) whose mean level was found decreased of more than two folds in T1D cells compared to the healthy counterpart: the majority of these genes (n=23) encoded for proteins functionally linked to the membrane, suggesting a rearrangement of the cell surface in T1D (Fig. 4f). Specifically, $T_{R3\text{-}56}$ cells from newly diagnosed T1D expressed lower levels of the G protein-coupled receptor 65 (GPR65) gene, that has been genetically associated with autoimmune disorders[31], KLRB1 (alias CD161) and KLRC1 (alias NKG2A), two killer cell lectin like receptors, described to function as inhibitory determinants in human NK cells [32,33]. Further, we also spotted in T1D $T_{R3\text{-}56}$ cells decreased expression of genes encoding for proteins related to regulatory functions, such as Lysosomal Protein Transmembrane 4 Beta (LAPTM4B)[34] and hydroxyprostaglandin dehydrogenase (HPGD)[35].

In summary, this study reveals that $T_{R3\text{-}56}$ cells may represent a disease biomarker with a previous undisclosed role in human T1D. In three independent cohorts - from Italy and Sweden - of new onset T1D subjects, we found that lower frequency of this cellular subset associates with reduced insulin-secreting capacity and with undesirable disease outcome,

such as DKA. Also, we found that $T_{R3\text{-}56}$ cells possess a certain degree of specificity for T1D as their enumeration failed to predict disease progression when T1D was preceded by another autoimmune disease as confounding factor. Moreover, $T_{R3\text{-}56}$ cells associated to C-peptide levels also later from T1D diagnosis (one year later), when metabolic alterations have been normalized. In all, our results also revealed functional, phenotypic and molecular impairments in $T_{R3\text{-}56}$ cells isolated at T1D onset suggesting a "general" dysregulation of this cellular subset in T1D, also confirmed by reduced expression of either inhibitory/activating receptors and of genes encoding for proteins involved in canonical T_{Reg} cell-mediated suppressive functions (i.e. LPTMB4 and HPGD)[32–35]. In an integrate view, defects of $T_{R3\text{-}56}$ cells associate with attack of pancreatic β-cells by islet-specific auto-reactive $CD8^+$ T cell clones, impacting on residual insulin production and influencing T1D progression (Extended Data 7). Further, $T_{R3\text{-}56}$ cell counts may represent a valuable criterion to monitor disease progression also improving stratification of individuals for T1D trials and identify at-risk pre-diabetic subjects during the asymptomatic phase of the disease. It is clear that more research is needed to further strengthen our findings, and studies are in progress also in other autoimmune disorders to expand the role of $T_{R3\text{-}56}$ cells in immunological self-tolerance and their potential translational relevance in a wider perspective. In conclusion, we propose a model in which in healthy conditions, $T_{R3\text{-}56}$ cells might participate to immune regulation to preserve tissue integrity of insulin-producing β-cells (Extended Data 7). An alteration in number and/or function of this cellular subset could lead to β-cell damage and loss of endogenous insulin production (measured as fasting C-peptide), thus allowing the seed of autoimmunity to take root (Extended Data 7).

Methods

Healthy and T1D subjects

Diagnosis of T1D was defined according to the Global International Diabetes Federation/International Society for Pediatric and Adolescent Diabetes Guidelines for Diabetes in Childhood and Adolescence[36] and included symptoms of diabetes in addition to casual plasma glucose concentration ≥11.1 mmol/L (200 mg/dl), or fasting plasma glucose ≥7.0 mmol/l (≥126 mg/dl), or 2 hours post load glucose ≥11.1 mmol/l (≥200 mg/dl) during an oral glucose tolerance test, and glycated haemoglobin (HbA_{1c}) ≥6.5[36]. Recent-onset T1D subjects and individuals one year after T1D diagnosis from Italian cohort were recruited at the Dipartimento di Scienze Mediche Traslazionali, Sezione di Pediatria, Università di Napoli “Federico II” (Prof. Adriana Franzese). T1D subjects from the validation Swedish cohort were recruited at Crown Princess Victoria Children´s Hospital, University Hospital, Linköping, Sweden (Prof. Johnny Ludvigsson); PBMCs were isolated and frozen at the Division of Pediatrics, Departement of Biomedical and Clinical Sciences, Linköping University, Sweden. Subjects from the cohort which developed other AIDs (CD or AIT) before or after T1D diagnosis were recruited at European Laboratory for the Investigation of Food-Induced Disease (ELFID), Università di Napoli “Federico II” (Prof. Riccardo Troncone). CD were diagnosed in accordance with the 1990 European Society for Pediatric Gastroenterology Hepatology and Nutrition guidelines[37]; diagnosis of AIT was based on the presence of high levels of antithyroid antibodies (anti-thyroperoxidase and/or anti-thyroglobulin), normal or low thyroid function (T4, TSH), together with a heterogenity and

hypoechogenity of thyroid parenchyma at ultrasound examination[38]. At-risk subjects, siblings of T1D children, were recruited at the Dipartimento di Scienze Mediche Traslazionali, Sezione di Pediatria, Università di Napoli “Federico II”. Autoantibody positive subjects were positive for at least two autoantibodies. Healthy children were recruited at the Dipartimento di Scienze Mediche Traslazionali, Sezione di Pediatria, Università di Napoli “Federico II” (Prof. Adriana Franzese). Blood samples from individuals with recent-onset T1D was achieved 10 d after glycaemic stabilization by treatment with exogenous insulin (glucose values between 3.5-10 mmol/l or 80-180 mg/dl) and all of them were positive for at least two anti-islet autoantibody. Healthy subjects were matched for sex, age and BMI with T1D subjects and selected by the following criteria: fasting blood glucose of <5.5 mmol/L (<100 mg/dl), negative personal and familial history of autoimmune disorders, and negativity for islet autoantibodies at the 99th percentile. T1D and healthy subjects with recent vaccinations or infections were excluded from the study. See Supplementary Tables 1-4 for demographic and clinical characteristics of T1D cohorts and healthy subjects.

Institutional Review Board of the Ethics Committee of University of Naples “Federico II” approved the study (Prot. N. 200/16 and N.161/18). Approval by the Research Ethics Committee by Linköping University was obtained (Dnr 02-482). All adult human subjects, or parents of participating children, provided written informed consent. We have complied with all relevant ethical regulations.

Laboratory testing

Blood samples from T1D subjects, at-risk siblings and from healthy individuals were withdrawn at 8.00 a.m. into heparinized BD Vacutainers and processed within the following 4 hours. Serum or plasma were obtained after centrifugation and kept at −80°C until use. Fasting C-peptide levels were measured in duplicate serum samples, at the same time for all samples, using a commercial ELISA kit (Merck Millipore Corporation). Results for each assay were validated, and a high- and low-level control sample were included. Glucose levels were measured using enzymatic hexokinase method and HbA1c by high-performance liquid chromatography (HLC-723 G7 TOSOH, Bioscience). Islet autoantibodies (GADA, IA-2A, IAA, ZnT8), transglutaminase IgA and antithyroid antibodies (anti-thyroperoxidase and/or anti-thyroglobulin) were measured by commercial ELISA (Pantec). Whole blood cells were analysed with a clinical-grade haemocytometer to determine absolute lymphocyte numbers in each sample. Remaining part of blood samples was processed and after Ficoll-Hypaque (GE-Healthcare) gradient centrifugation, PBMCs were obtained.

For the validation T1D Swedish cohort, blood samples were processed at Division of Pediatrics, Department of Clinical and Experimental Medicine, Medical Faculty Linköping University, Sweden. PBMCs were obtained and cryopreserved in liquid nitrogen. An aliquot of them were shipped to our laboratory at IEOS-CNR and kept in liquid nitrogen until use. Nitrogen cryopreserved PBMCs from Swedish cohort were thawed as follows: cryovials containing frozen cells were removed from liquid nitrogen storage and placed into a 37°C water bath; the vials were gently swirling in the 37°C water bath until there was a small amount of ice left in the vial. Pre-warmed complete growth medium (RPMI 10% FBS) drop

wise into the cryovial containing the thawed cells. After centrifugation cells were re-suspend in complete growth medium and utilized for flow cytometry staining. Viability was always assessed after defrosting and was on average > 85%.

Flow cytometry and cell isolation

PBMCs from human healthy donors, T1D subjects and at-risk siblings of T1D were stained with the following antibodies for the evaluation of $T_{R3\text{-}56}$ cells: FITC anti-human CD3 (BD Pharmingen, clone UCHT1), PE-Cy7 anti-human CD56 (BD Pharmingen, clone B159).

For the evaluation of $T_{R3\text{-}56}$ death cell, PBMCs were stained with the following antibodies: FITC human Annexin V (BD Pharmingen), PE-Cy7 anti-human CD56 (BD Pharmingen, clone B159), APC anti-human CD3 (BD Pharmingen, clone UCHT1), propidium iodide (BD Pharmingen); Annexin V buffer (BD Pharmingen) was used for the staining according the manufactories' instructions.

Multiparametric flow cytometry were used for the evaluation of surface markers on $T_{R3\text{-}56}$ cells from PBMCs: FITC or APC anti-human CD3 (BD Pharmingen, clone UCHT1), PE or APC-H7 anti-human CD4 (BD Pharmingen, clone RPA-T4), BV421 anti-human CD8 (BD Pharmingen, clone RPA-T8), PE anti-human CD16 (BD Pharmingen, clone 3G8), BV510 anti-human CD27 (BD Pharmingen, clone M-T271), PE anti-human CD28 (BD Pharmingen, clone CD28.2), APC anti-human CD45 (BD Pharmingen, clone HI30), FITC anti-human CD45RA (Miltenyi Biotec, clone REA562), APC anti-human CD45RO (BD Pharmingen, clone UCHL1), PeCy7 or APC anti-human CD56 (BD Pharmingen, clone B159; BD Biosciences, clone NCAM16.2), APC anti-human CD94 (BD Pharmingen, clone HP-3D9), BB700 anti-human CCR7 (BD Horizon, clone 3D12), BV510 anti-human CXCR3 (BD Optibuild, clone 1C6/CXCR3), BB700 anti-human CXCR4 (BD Horizon, clone 12G5), BV510 anti-human DNAM-1 (BD Optibuild, clone DX11), BB700 anti-human NKG2A (BD Optibuild, clone 131411), BV510 anti-human NKG2C (BD Optibuild, clone 134591), APC anti-human NKG2D (BD Pharmingen, clone 1D11), PE labelled CD1d tetramers loaded with α-galactosyl ceramide (ProImmune), PE labelled CD1d negative control tetramers (ProImmune), FITC anti-human Vα24 (Beckman Coulter, clone C15), BV421 anti-human Granzyme B (BD Horizon, clone GB11), PECy7 anti–human CD25 (BD Pharmingen, clone M-A251), BV421 anti–human PD-1 (BD Horizon, clone EH12-1), PE anti-human FoxP3-all (BD Pharmingen, clone 259D/C7), APC anti–human CD152/CTLA-4 (BD Pharmingen, clone BN13), APC anti-human CD39 (BD Pharmingen, clone TU66), BV421 anti-human GITR (BD Horizon, clone V27-580). FITC and PE labelled mAbs against TCR Vβ epitopes; anti-human Vβ1, Vβ2, Vβ3, Vβ4, Vβ5.1, Vβ5.2; Vβ5.3, Vβ7.1, Vβ7.2, Vβ8, Vβ9, Vβ11, Vβ12, Vβ13.1, Vβ13.2, Vβ13.6, Vβ14, Vβ16, Vβ17, Vβ18, Vβ20, Vβ1.3, Vβ22 and Vβ23 all from Beckman Coulter. Granzyme B expression was performed by using the fixation/permeabilization solution kit BD Cytofix-Cytoperm (BD Biosciences), according the manufacturer's instructions. Staining for intracellular factors was performed by using fixation and permeabilization FoxP3 buffer kit (BD Pharmingen), according the manufacturer's instructions. Samples were acquired by using a two lasers equipped FACSCanto II (BD Bioscience); at least $3x10^4$ events in the lymphocyte gate. For the evaluation of positive events, fluorescence minus one (FMO) controls were used for

Europe PMC Funders Author Manuscripts

setting the gate; non-viable cells were detected by 7-AAD viability staining (BD Pharmingen). See Supplementary Figure 1 for gating strategy of $T_{R3\text{-}56}$ cells. Cytofluorimetric analyses were performed by using FlowJo Software (FlowJo, LLC).

Human $CD3^+CD56^+$ ($T_{R3\text{-}56}$), $CD3^-$ $CD56^+$ (NK), $CD3^+CD56^-$, $CD4^+$ and $CD8^+$ T cells were isolated from PBMCs of human healthy donors and T1D subjects by high-performance cell sorting (BD FACS-Jazz, BD Bioscience) in the IEOS-CNR Sorting Facility in Naples, after staining with the following antibodies: FITC anti-human CD3 (BD PharMingen, clone UCHT1), APC anti-human CD56 (BD Biosciences, clone NCAM16.2), APC anti-human CD4 (BD Pharmingen, clone RPA-T4), APC anti-human CD8 (BD Pharmingen, clone RPA-T8) or by magnetic cell separation with microbeads $CD3^+CD56^+$ isolation Kit (Miltenyi Biotec), Dynabeads™ CD8 Positive Isolation Kit (Invitrogen, Thermo Fisher Scientific) and Dynabeads™ Regulatory $CD4^+CD25^+$ T Cell Kit for $CD4^+$ cell isolation (Invitrogen, Thermo Fisher Scientific). Purity of isolated cells was 95%-99% as reported in figures.

Proliferation assays

To analyse cell division, flow-sorted $CD4^+$ and $CD8^+$ T cells were labelled with 5,6-carboxyfluorescein-diacetate-succinimidyl ester (CFSE) (Thermo Fischer Scientific) before the culture[39]. For the assessment of cell proliferation, $3x10^4$ $CD4^+$ or $CD8^+$ cells were cultured for 72 hours in the presence of $T_{R3\text{-}56}$ cells (or $CD3^+CD56^-$ control cells) stimulated with anti-CD3 plus anti-CD28 microbeads (0.2 beads/cell) (Gibco, Thermo Fisher Scientific) at different cell *ratio* (1:1, 1:2, 1:4, 1:8), as previously indicated[39]. All tests were performed in the presence of RPMI 1640 medium supplemented with 5% heat inactivated AB human serum (Euroclone). CFSE analyses were performed using BD FACSCanto II (BD Biosciences) and FlowJo software V.10 (FlowJo, LLC).

Cytotoxicity assays

To obtain CTLs directed against allogeneic targets, flow sorted $CD8^+$ cells (purity > 95%) from adult healthy donor (effectors) were cultured with 30 Gy-irradiated allogeneic PBMCs (stimulators) for 10 days with regular hrIL-2 supplementation (20 IU/ml); allogeneic targets were obtained by anti-CD3 treatment and hrIL-2 expansion of stimulator PBMCs; specific cytotoxicity of effector cells was measured by using the 5,6-carboxyfluoresceindiacetate (CFDA) cytotoxicity assay (Molecular Probes, Eugene). Briefly, the target cells were labelled with CFDA mixed with effector cells at different E:T *ratio* and incubated at 37°C for 3 hours in 96-well round-bottom plates (Falcon, Becton Dickinson). The specific lysis of target cells was calculated as follows: % specific lysis = (CT-TE/CT) x100, where CT indicates mean number of fluorescent target cells in control tubes and TE indicates mean number of fluorescent cells in target plus effector tubes[40,41]. $T_{R3\text{-}56}$ cells (or $CD8^+$ control cells) and effector CTLs were co-cultured (at 1:1 ratio) in order to evaluate the ability of $T_{R3\text{-}56}$ cells to suppress lytic capacity of effector CTLs against the CFDA-labeled allogeneic target (see experimental procedure Supplementary Fig. 3).

Degranulation assay, CD107/LAMP-1 expression and IFN-γ production

To obtain activated CTLs, flow-sorted $CD8^+$ T cells were cultured for 36 hours in RPMI-1640 (Gibco, Life Technologies) supplemented with 5% AB human serum

(Euroclone) in the presence of hrIL-2 (Roche) at 200 IU/ml. After 36 hours, CTLs were labelled with BV421-conjugated anti-human CD8 and then cultured alone or in the presence of freshly flow-sorted $T_{R3\text{-}56}$, NK and $CD8^+$ T lymphocytes at different ratio, with or without TCR-stimulation (1 bead/cell) in 96-well round-bottom plates (Falcon, Becton Dickinson). PE-conjugated anti-human CD107a/LAMP-1 (BD Pharmingen, clone H4A3) was added to the cell culture for the whole culture period (4 hours).

To avoid extracellular cytokine export, the cultures were performed in the presence of 5 μg/ml of Brefeldin-A (Sigma-Aldrich), as described[42]; in particular for CD107a/LAMP-1 experiments Brefeldin-A was added in the last 3 hours of culture. For IFN-γ production, CTLs were cultured as described above, while 5 μg/ml of Brefeldin-A was added to the cell culture for the whole culture period (4 hours)[12,13,42]. Then to evaluated IFN-γ expression, samples were fixed and permeabilized (Cytofix-Cytoperm, BD Bioscience) and stained for PE-conjugated anti-human IFN-γ (BD Pharmingen, clone B27), following the manufacturer's instructions.

For transwell experiments, the co-culture of $T_{R3\text{-}56}$ cells with CTLs was performed in the above condition using transwell inserts (Corning Life Sciences) in 24-well round-bottom plates (Falcon, Becton Dickinson). For the degranulation assay in the presence of CD56 blocking soluble human recombinant cell adhesion molecule NCAM-1/CD56 (R&D Systems Inc.) was used (10 ng/ml). The control 345.134 IgG2a mAb, recognizing a glycoprotein widely expressed on human leucocytes[43] was a kind gift of Dr. S. Ferrone, and was used as described above.

In all the experiments, non-viable cells were detected by 7-AAD viability staining and both CD107a/LAMP-1 expression and IFN-γ production were evaluated in labelled-CTLs, using fluorescence values of unstimulated CTLs (medium) as negative values to identify positive gate, as described in experimental procedure in Supplementary Figure 4 and gating strategy in Supplementary Figure 5. All the experiments were performed in autologous condition except when indicated. Experiments in adult healthy subjects were performed co-culturing $1x10^5$ CTLs and $1x10^5$ $T_{R3\text{-}56}$ or control cells; experiments in T1D and control children were performed co-culturing at least $3x10^4$ CTLs and $3x10^4$ $T_{R3\text{-}56}$ or control cells due to the reduced volume of blood withdrawn from children and also due to the reduce frequency of this population in T1D.

ROS production

For intracellular ROS production CTLs were stained using 2',7'-dichlorodihydrofluorescein diacetate (DCF) (Sigma-Aldrich). Briefly, CTLs were stained with DCF and cultured alone or with $T_{R3\text{-}56}$ or control cells in the presence of anti-CD3 plus anti-CD28; ROS production was detected after 5, 20 e 40 min of culture. Induction of intracellular ROS was obtained by treating CTLs with menadione (0.05 μM). Mitochondrial ROS was measured by MitoSOX Red Mitochondrial Superoxide Indicator (Thermo Fisher Scientific), according to manufactore's instructions. DCF and mitoSoX levels were evaluated by flow cytometry using BD FACSCanto II (BD Biosciences) and FlowJo software (FlowJo, LLC).

Seahorse analyses

Metabolic profile was evaluated in T_{R3-56}, NK, $CD3^+CD56^-$ and $CD8^+$ cells from adult healthy subjects, in the presence of anti-CD3 plus anti-CD28 microbeads (1 bead/cell) (Gibco, Thermo Fisher Scientific) for 1 hour. Real time measurements of extracellular acidification rate (ECAR) and oxygen consumption rate (OCR) were performed by an XFe-96 Analyzer (Agilent Technologies). Specifically, cells were plated in XFe-96 plates (Agilent Technologies) at the concentration of 2 x 10^5 cells/well and cultured with RPMI-1640 medium supplemented with 5% AB human serum. ECAR was measured in XF DMEM medium (Agilent Technologies) in basal condition and in response to 10 mM glucose, 5 μM oligomycin and 100 mM of 2DG (all from Sigma-Aldrich). OCR was measured in XF DMEM medium (supplemented with 10 mM glucose, 2 mM L-glutamin, and 1 mM sodium pyruvate), under basal conditions and in response to 5 μM oligomycin, 1.5 μM of carbonylcyanide-4-(trifluoromethoxy)-phenylhydrazone (FCCP) and 1 μM of antimycin A and rotenone (all from Sigma-Aldrich). Experiments with the Seahorse were done with the following assay conditions: 3 minutes mixture; 3 minutes wait; and 3 minutes measurement.

Transcriptome analysis

For microarray analysis flow sorted cell populations (T_{R3-56}, NK, $CD3^+CD56^-$, $CD8^+$ isolated were isolated from helathy adults (n=3 biological replicates for each cell population obtained from adult healthy individuals) were quantified through microarray-based human Affymetrix Clariom S Assays (Eurofins Genomics), which provides extensive coverage of all known well-annotated genes (21448 gene probes for 19525 annotated unique genes). The raw intensity values were background corrected, log2 transformed and quantile normalized using the Robust Multi-array average (RMA) algorithm. Data were imported and analysed using MultiExperimentViewer (MeV). Sample similarity was described by multivariate Principal Component Analysis (PCA) and Pearson's correlation. For supervised sample clustering, significant genes were selected by one-way ANOVA, followed by Pearson's correlation. In order to identify a T_{R3-56} cell specific gene expression pattern, we selected genes for having a consistent log2 fold change (either > +1 or < -1) compared to all other evaluated populations (NK, $CD3^+CD56^-$ and $CD8^+$ cells) and a significant Student's *t*-test ($p<0.05$) for all three comparisons: T_{R3-56} *vs* NK, T_{R3-56} *vs* $CD3^+CD56^-$ and T_{R3-56} *vs* $CD8^+$ T cells.

For NGS analysis, RNA sequencing was performed by IGA technology (IGATech) services (Udine, Italy). Total RNA was extracted from T_{R3-56} cells isolated from either healthy subjects (n=3) or recent-onset T1D subjects (n=3) using the RNeasy Micro Kit from QIAGEN, according to manufacturer's instructions. RNA samples were then quantified and quality tested by Agilent 2100 Bioanalyzer RNA assay (Agilent technologies, Santa Clara, CA) or Caliper (PerkinElmer, Waltham, MA). Libraries were prepared by the 'Ovation SoLo RNA-seq Library Preparation kit' (NuGEN, San Carlos, CA), following the manufacturer's instructions and checked with both Qubit 2.0 Fluorometer (Invitrogen, Carlsbad, CA) and Agilent Bioanalyzer DNA assay or Caliper (PerkinElmer, Waltham, MA). Sequencing was performed on single-end 75 bp mode on NextSeq 500 (Illumina, San Diego, CA) and number of reads ranged from 29.1x10^6 to 32.5x10^6. Raw data were processed by Bcl2Fastq

2.0.2 version of the Illumina pipeline for both format conversion and de-multiplexing and lower quality bases and adapters were removed by ERNE Version 1.4.6[44] and Cutadapt 1.16[45] software. Reads were then deduplicated based on unique molecular identifier (UMI) composed of 8 random bases for unambiguous identification of unique library molecules by IGATech proprietary script; and aligned on reference GRCh38 genome/transcriptome with STAR3 2.6[46]. Full-length transcripts representing multiple spliced variants for each gene locus were assembled and quantified by Stringtie 1.3.4d[47]. RNA-Seq data was preprocessed by counting the overlap of reads with genes through htseq-count 0.9.1[48] and DESeq2 1.14.1[49] was used to perform comparisons between expression levels of genes and transcripts. Normalization was performed using the median-of-ratios method[50] and statistical significance determined using a Wald test[49].

Cytokine assessment

A total of 40.000 flow-sorted $T_{R3\text{-}56}$ cells from healthy and T1D subjects were cultured with RPMI-1640 medium supplemented with 5% serum autologous in the presence of anti-CD3 plus anti-CD28 microbeads (0.1 bead/cell) (Gibco, Thermo Fisher Scientific). After 48 hours supernatant were collected and stored at -20° C until use. Cytokine production was analyzed using the bead-based multianalyte immunoassay (Invitrogen, Thermo Fisher Scientific) according to the manufacturer's recommendations, and then was measured by Multiplex technology (Luminex 200, Luminex). xPONENT 3.1 software (Luminex) was used for data acquisition.

Statistical analysis

Modelling and statistical analyses of data were carried by *JMP Statistical Discovery* software 6.0.3 (SAS, North Carolina, USA), and *GraphPad Prism 7 software* (GraphPad, California, USA). Comparisons were performed by Mann-Whitney U-test, Student's *t*-test, one-way ANOVA and two-way ANOVA-corrected for multiple comparison using Bonferroni test and Wilcoxon matched pairs test as indicated. Correlation analyses were performed by Pearson's correlation. A linear model was used for the adjustment of the comparison for sex, age and BMI variables. To identify outliers, ROUT (Q=0.1%) method has been applied.

For all analyses, we used two-tailed tests, with $p<0.05$ values denoting statistical significance. A univariate logistic regression modeling was fitted to predict DKA at T1D diagnosis as described: T1D subjects were dichotomized on the basis of the presence (Yes) or absence (No) of DKA at disease diagnosis. Prognostic validity of the fitted models was evaluated by receiver operating characteristic (ROC) curve analysis and measured using the area under the ROC curve (AUC). The black line represents the ROC curve that derives from sensitivity (the probability that X value is true positive) versus 1-specificity (the probability that X value is false positive). The yellow line indicates the optimal combination of sensitivity and specificity according to the Youden criterion. The optimal combination between sensitivity and specificity is represented by the interception between the ROC curve and the yellow line.

Extended Data

Europe PMC Funders Author Manuscripts

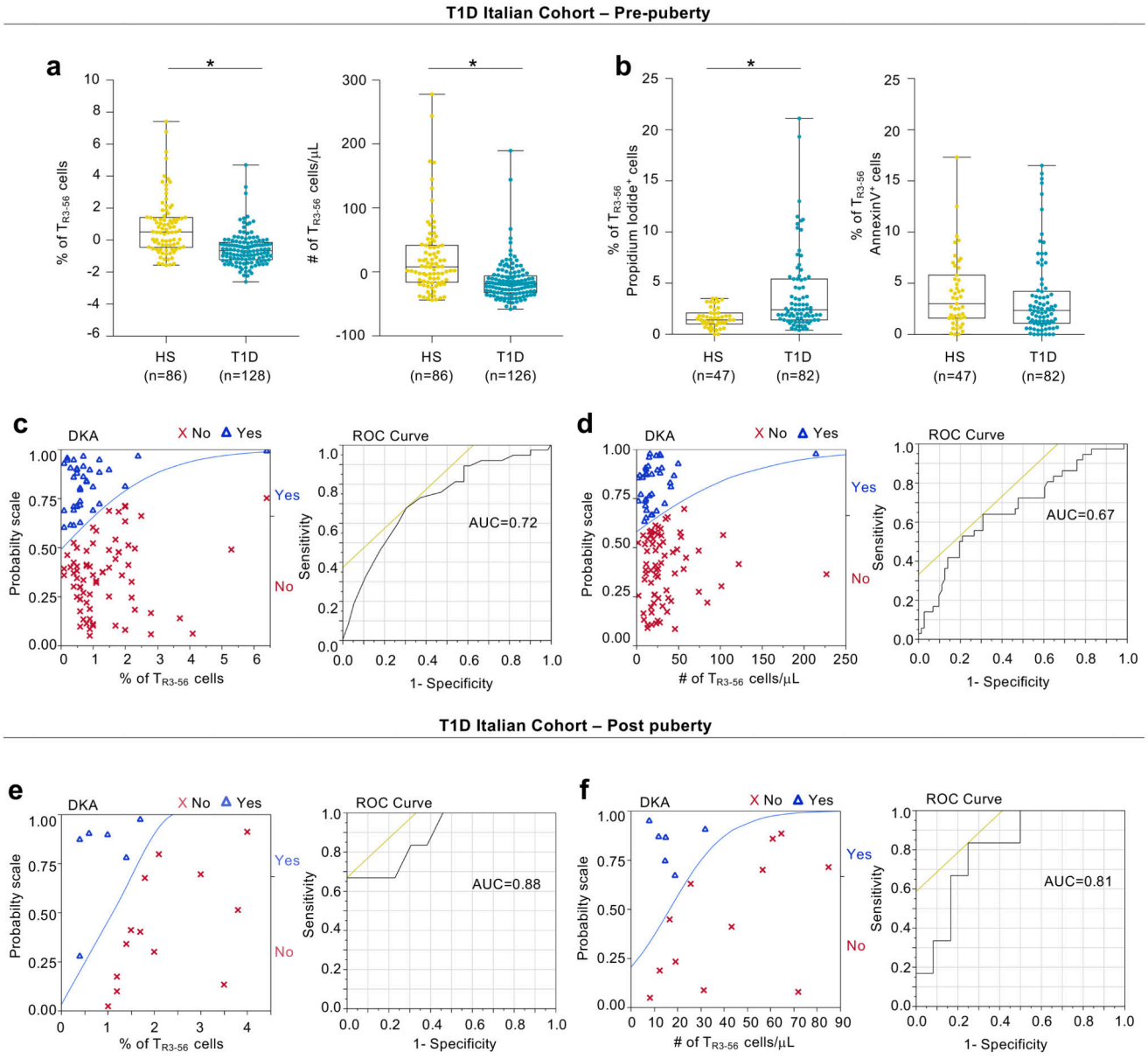

Extended Data Fig. 1. $T_{R3\text{-}56}$ cell enumeration predicts residual β-cell function and DKA in pre-puberty T1D subjects at disease onset.

a, Box plots indicate the percentage (left) and absolute number (right) of circulating $T_{R3\text{-}56}$ cells in pre-puberty T1D subjects at disease onset from Italian cohort compared with healthy subjects, after adjustment for age, sex and BMI. Data are presented as box plots (min, max, median, and 25th and 75th percentiles), each dot represents a individual subjects (n=86 healthy subjects; n=128 T1D for percentage of $T_{R3\text{-}56}$ cells and n=126 T1D for absolute number of $T_{R3\text{-}56}$ cells). *p<0.0001 by two-tailed Mann-Whitney U-test. **b**, Box plots

indicate the percentage of necrotic (left) and apoptotic (right) rate of circulating $T_{R3\text{-}56}$ cells in healthy subjects (n=47) and T1D children at disease onset (n=82) from Italian cohort. Data are presented as box plots (min, max, median, and 25th and 75th percentiles), each dot represents a individual subjects. *p<0.0001 by two-tailed Mann-Whitney U-test. **c**, Left, logistic regression modeling shows that percentage of $T_{R3\text{-}56}$ cells predicts the presence or absence of DKA in pre-puberty T1D subjects at diagnosis (n=128) from Italian cohort. T1D subjects were dichotomized on the basis of the presence (Yes) or absence (No) of DKA at disease diagnosis. Low numbers of $T_{R3\text{-}56}$ cells at diagnosis associated with presence of DKA. Right, ROC curve of the model-based prognostic scores of $T_{R3\text{-}56}$ cells for the presence of DKA. AUC=0.72. **d**, Left, logistic regression modeling shows that absolute number of $T_{R3\text{-}56}$ cell counts predicts the presence or absence of DKA in pre-puberty T1D subjects at diagnosis (n=126) from Italian cohort. Right, ROC curve of the model-based prognostic scores of $T_{R3\text{-}56}$ cells for the presence of DKA. AUC=0.67. **e**, Left, logistic regression modeling shows that percentage of circulating $T_{R3\text{-}56}$ cells predicts the presence or absence of DKA in post-puberty young adults T1D (n=19) from Italian cohort. Right, ROC curve of the model-based prognostic scores of $T_{R3\text{-}56}$ cells for the presence of DKA. AUC=0.88. **f,** Left, logistic regression modeling shows that absolute number of $T_{R3\text{-}56}$ cells predicts presence of DKA in post-puberty young adults T1D (n=18) from Italian cohort. Right, ROC curve of the model-based prognostic scores of $T_{R3\text{-}56}$ cells for the presence of DKA. AUC=0.81.

Europe PMC Funders Author Manuscripts

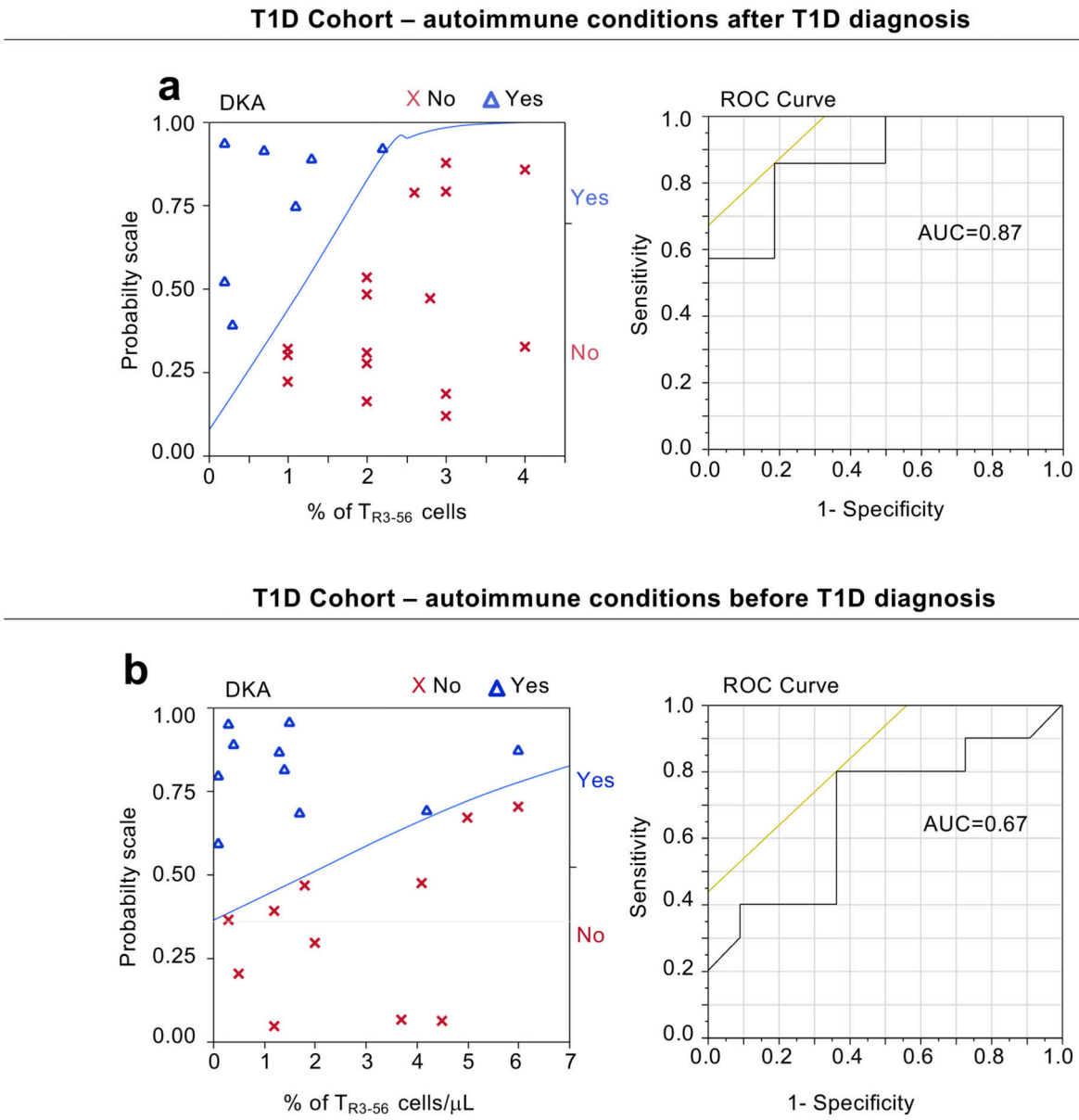

Extended Data Fig. 2. T_{R3-56} cells in T1D subjects with other autoimmune diseases.

a, Left, logistic regression modeling shows that percentage of T_{R3-56} cells predicts the presence or absence of DKA in children (n=23) that developed after diagnosis of T1D another autoimmune conditions (CD or AIT). T1D subjects were dichotomized on the basis of the presence (Yes) or absence (No) of DKA at disease diagnosis. Right, ROC curve of the model-based prognostic scores of T_{R3-56} cells for the presence of DKA. AUC=0.87. **b**, Left, logistic regression modeling shows that peripheral frequency of T_{R3-56} cells associated with presence of DKA in children (n=21) that at T1D diagnosis are already affected by other autoimmune conditions. Right, ROC curve of the model-based prognostic scores of T_{R3-56} cells for the presence of DKA. AUC=0.67.

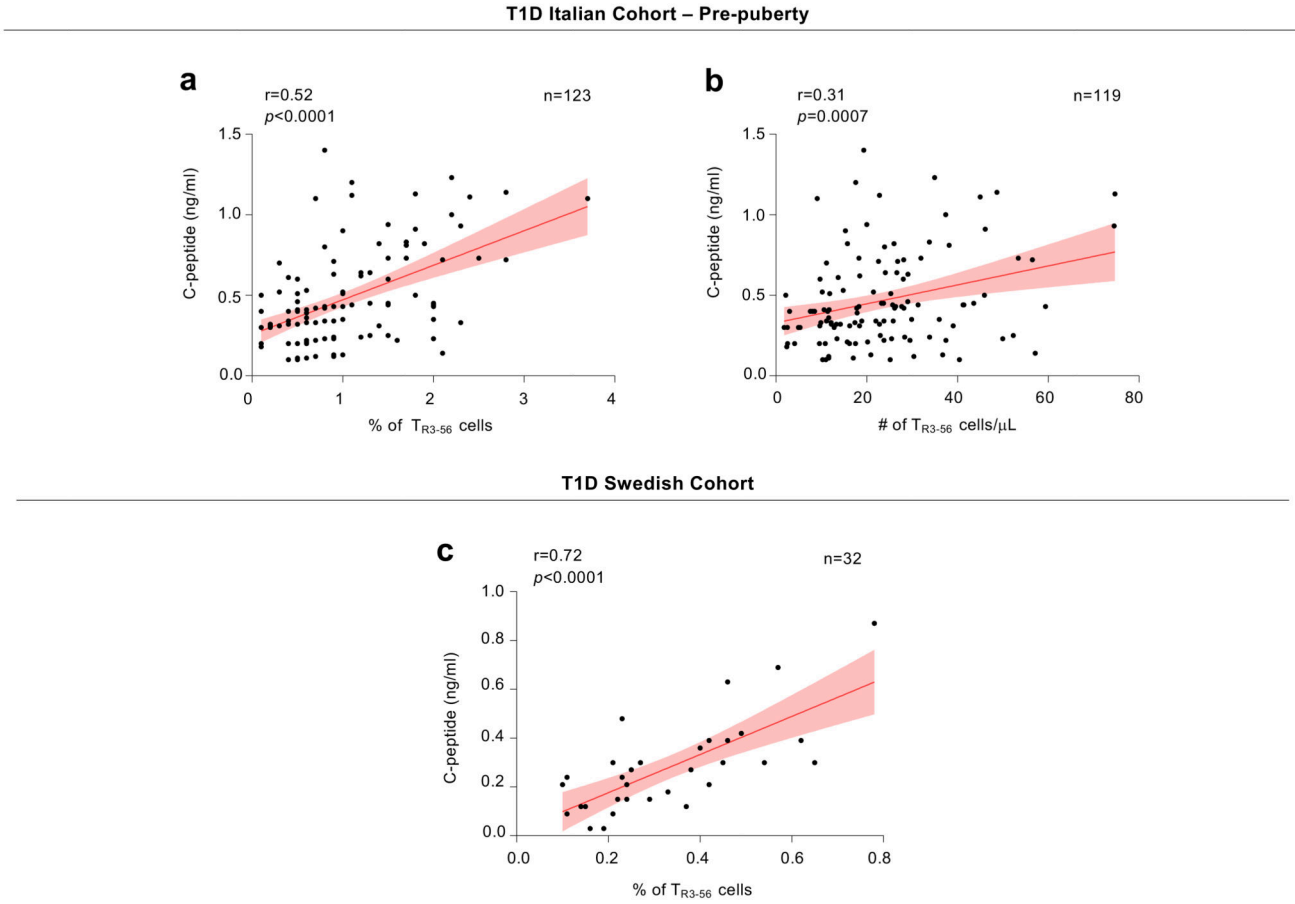

Extended Data Fig. 3. Correlation between $T_{R3\text{-}56}$ cells and fasting C-peptide in the absence of outliers.

a, Scatter plot showing statistical correlation between frequency of $T_{R3\text{-}56}$ cells and fasting C-peptide in the absence of $T_{R3\text{-}56}$ cell outliers (n=5) in pre-puberty T1D subjects (n=123) at disease onset from Italian cohort. Red line indicates regression line and shading indicates confidence interval. r=0.52, p<0.0001 by two-tailed Pearson's correlation. **b**, Scatter plot showing statistical correlation between absolute numbers of $T_{R3\text{-}56}$ cells and C-peptide in the absence of $T_{R3\text{-}56}$ cell outliers (n=7) in pre-puberty T1D subjects (n=119) at disease onset from Italian cohort. Red line indicates regression line and shading indicates confidence interval. r=0.31, p=0.0007 by two-tailed Pearson's correlation. **c**, Scatter plot showing positive correlation between the frequency of circulating $T_{R3\text{-}56}$ cells and serum levels of fasting C-peptide in absence of $T_{R3\text{-}56}$ outliers (n=4) in Swedish cohort of T1D children (n=32) at disease onset; Red line indicates regression line and shading indicates confidence interval. r=0.72, p<0.0001 by two-tailed Pearson's correlation. To identify outliers ROUT (Q=0.1%) method has been applied.

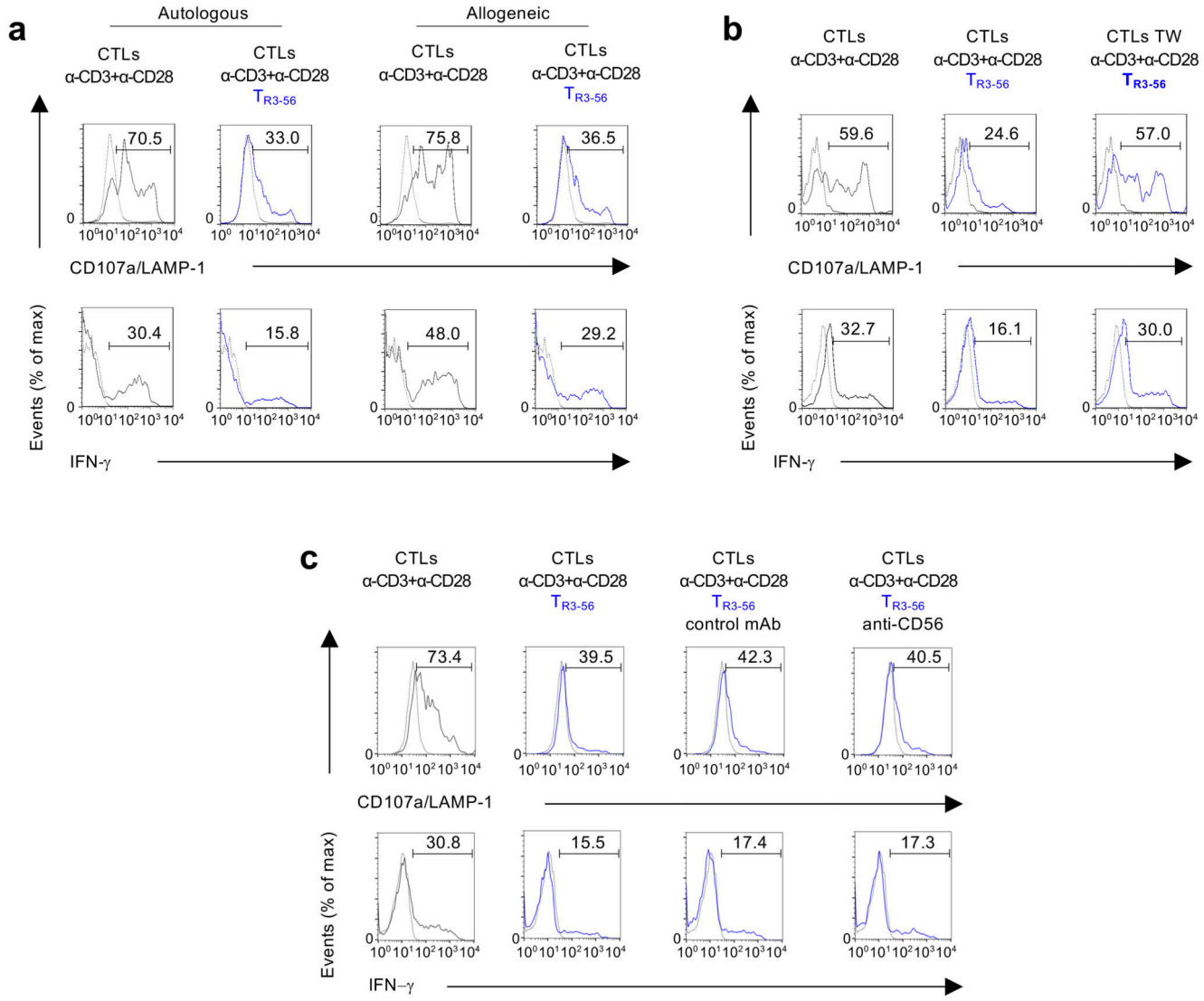

Extended Data Fig. 4. T_{R3-56} cells suppress CD107a/LAMP-1 and IFN-γ in both autologous and allogeneic conditions, require cell-to-cell contact and is independent from CD56 molecules.

a, Representative flow cytometry histograms showing CD107a/LAMP-1 and IFN-γ staining of CTLs after 4 hours of culture with anti-CD3 plus anti-CD28 microbeads alone (grey), in the presence of autologous or allogeneic T_{R3-56} cells (blue) as indicated. Dotted lines indicate unstimulated CTLs. Numbers indicate percentage of positive cells. Data are from one representative experiment out of four. **b**, Representative flow cytometry histograms showing CD107a/LAMP-1 and IFN-γ staining of CTLs cultured for 4 hours with anti-CD3 plus anti-CD28 microbeads alone (grey), in the presence of T_{R3-56} cells or when T_{R3-56} cells were separated by transwell (TW) plate system (as indicated). Dotted lines indicate unstimulated CTLs. Numbers indicate percentage of positive cells. Data are from one representative experiment out of six. **c**, Representative flow cytometry histograms showing CD107a/LAMP-1 and IFN-γ staining of CTLs after 4 hours of culture with anti-CD3 plus anti-CD28 microbeads alone (grey), or in the presence of T_{R3-56} cells (blue), either in the

Europe PMC Funders Author Manuscripts

presence of the control 345.134 IgG2a or the anti-CD56 neutralizing mAb, as indicated. Dotted lines indicate unstimulated CTLs. Numbers indicate percentage of positive cells. Data are from one representative experiment out of three.

Europe PMC Funders Author Manuscripts

Europe PMC Funders Author Manuscripts

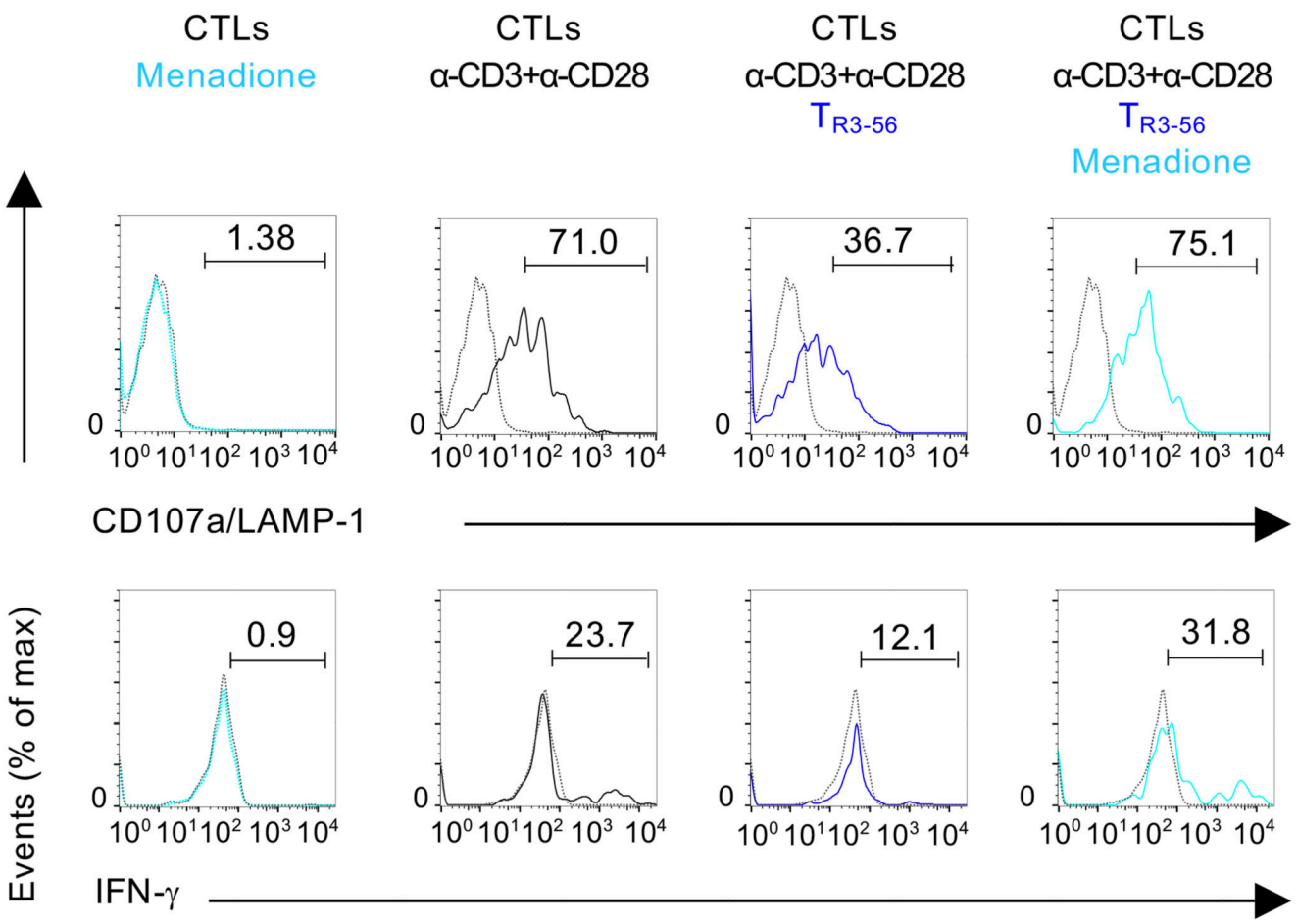

Extended Data Fig. 5. Menadione pre-treated CTLs are resistant to T_{R3-56} cell suppressive activity.

CD107a/LAMP-1 and IFN-γ staining of CTLs cultured for 4 hours in the presence or absence of anti-CD3 plus anti-CD28 microbeads alone or in the presence of T_{R3-56} cells; light blue lines indicate CTLs pre-treated for 15 minutes with 0.05 mM menadione. Dotted lines indicate unstimulated cells. Numbers indicate percentage of positive cells. Data are from one representative experiment out of six.

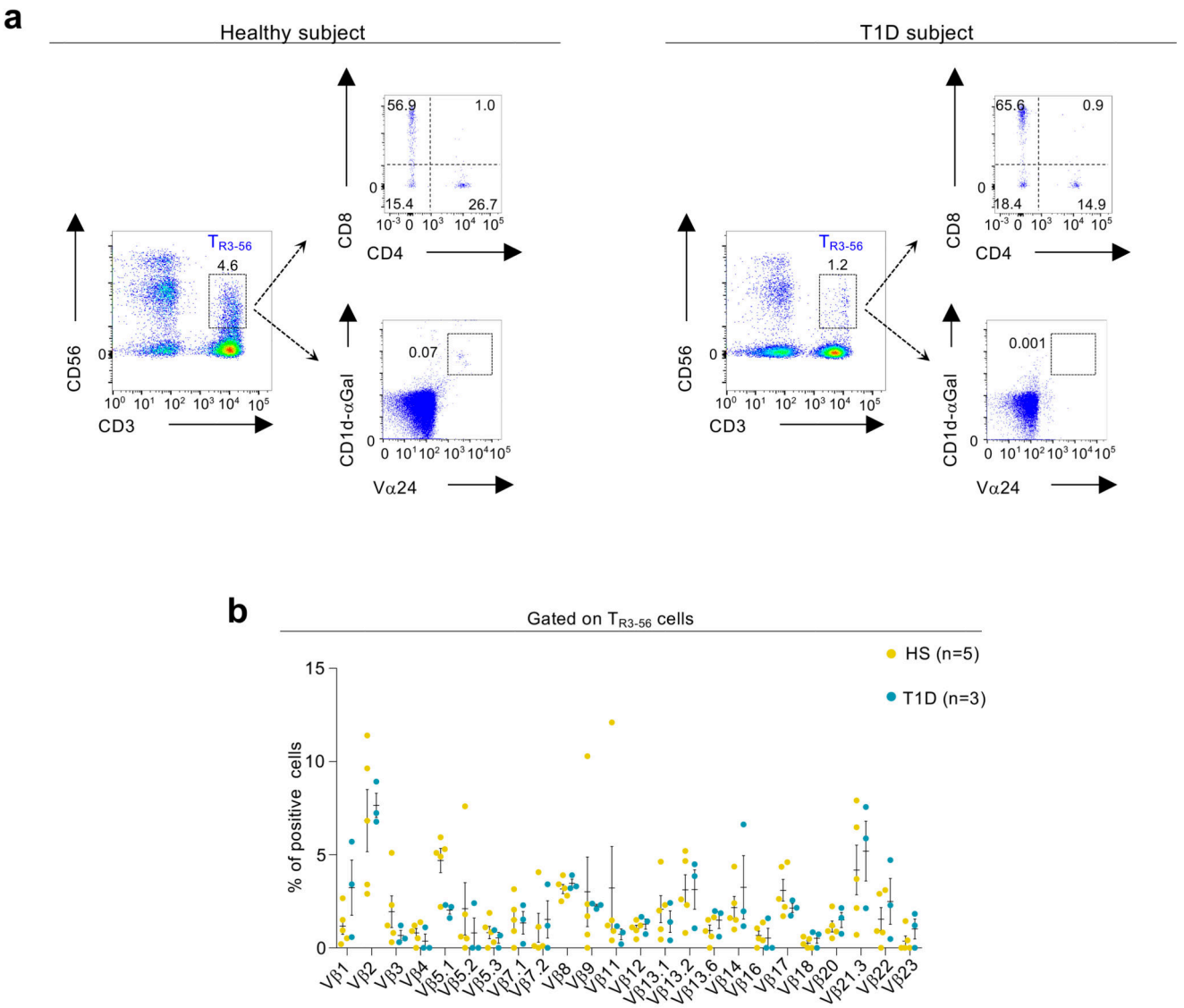

Extended Data Fig. 6. Phenotype of peripheral T_{R3-56} cells in healthy and T1D subjects.

a,Representative flow-cytometry plots showing the gating strategy used to evaluate the expression of CD4 and CD8 on T_{R3-56} cells (upper panels) and the frequency of invariant (i)NKT cells, evaluated by Vα24 expression and CD1d tetramers loaded with a-Galactosyl ceramide (CD1d-aGal) binding on T_{R3-56} lymphocytes (lower panels) on both healthy and T1D at-onset subjects, as indicated. Numbers in plots indicate percent of positive cells. **b**, Column bar showing the TCR Vβ family expression in T_{R3-56} cells from healthy subjects (yellow) and T1D children (turquoise) at diagnosis, as indicated. Data are from n=5 healthy subjects and n=3 T1D subjects. Data are expressed as mean ± SEM. No statistical significance differences are identified by two-way ANOVA-corrected for multiple comparison using Bonferroni test ($p > 0.9999$).

Europe PMC Funders Author Manuscripts

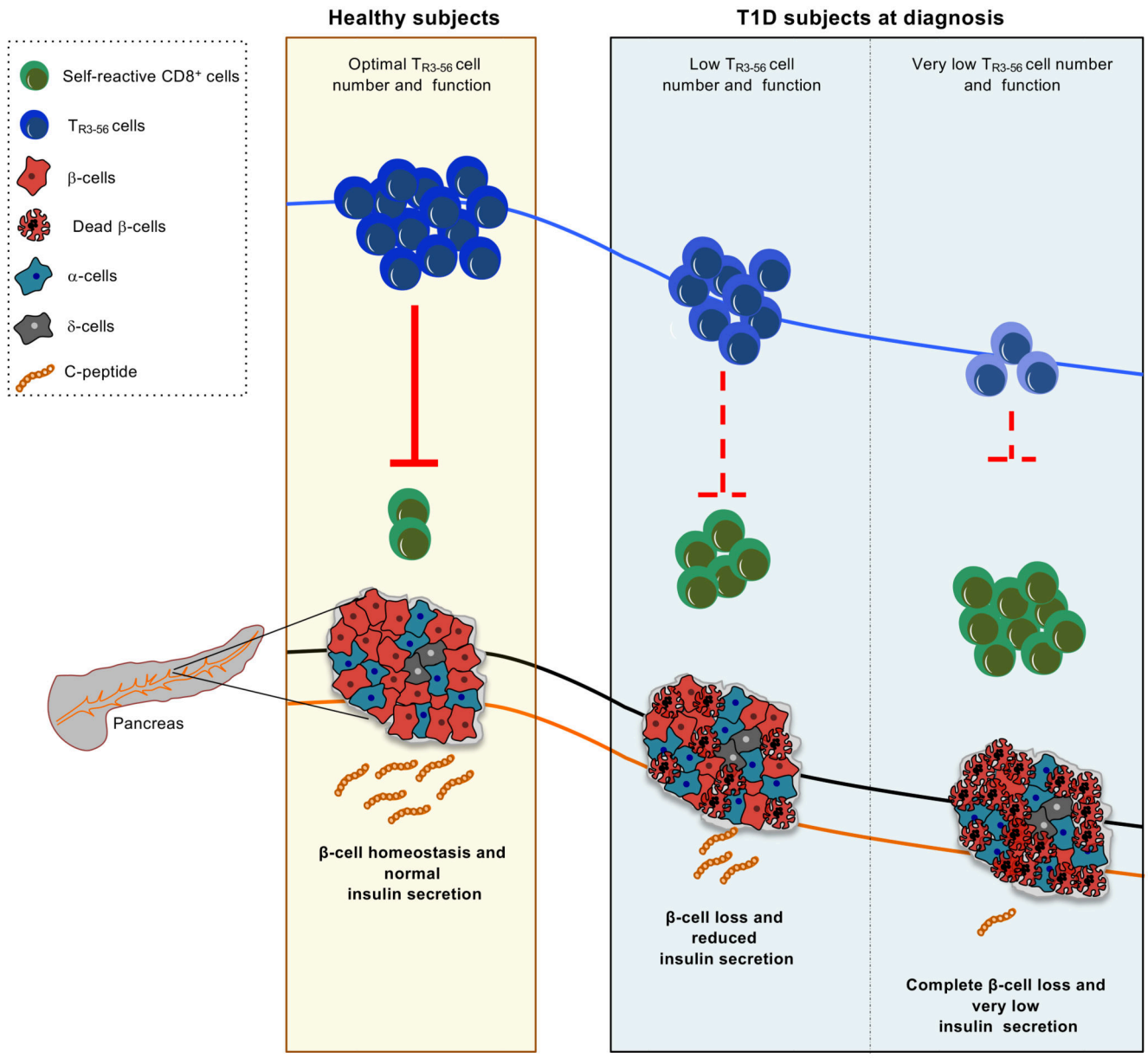

Extended Data Fig. 7. Hypothetic model showing the regulatory function of T_{R3-56} cells and β-cell integrity in healthy and autoimmune conditions.

In healthy subjects, normal number and suppressive function of T_{R3-56} cells control self-reactive $CD8^+$ T cells (green), possible contributing to maintenance of immune self-tolerance and insulin production by live β-islet cells (red). Right, in autoimmune T1D, a lower frequency and a reduced functional capacity of T_{R3-56} cells correlated with reduced β-cell mass, reduced serum levels of C-peptide and progressive lost of immunological self-tolerance. The schematic model was prepared using the Motifolio Scientific Illustration Toolkit.

Supplementary Material

Refer to Web version on PubMed Central for supplementary material.

Acknowledgements

We thank M. Montagna and all members of the IEOS-CNR for technical support. M. Carrara and F. Marabita for assistance in transcriptomic analysis. This paper was supported by grants from the Juvenile Diabetes Research Foundation (JDRF n. 2-SRA-2018-479-S-B to M.G.; JDRF n. 1-SRA-2018-477-S-B to P.d.C); the European Foundation for the Study of Diabetes (EFSD/JDRF/Lilly Programme 2016 to M.G.); the National Multiple Sclerosis Society (NMSS n. PP-1804-30725 to M.G.); Fondazione Italiana Sclerosi Multipla (FISM n. 2016/R/18 to G.M.; FISM n. 2018/R/4 to V.D.R.); by Ministero della Salute (n. GR-2016-02363725 to V.D.R); Università degli Studi di Napoli “Federico II” (STAR Program Linea 1 - 2018 to V.D.R.); European Research Council Grant (ERC "menTORingTregs" n. 310496 to G.M.); Telethon (n. GGP 17086 to G.M.); Italian Ministry of Health Giovani Ricercatori (n. GR-2016-02363749 to C.Pr.).

References

1. Liblau RS, Wong FS, Mars LT, Santamaria P. Autoreactive CD8 T cells in organ-specific autoimmunity: emerging targets for therapeutic intervention. Immunity. 2002; 17:1–6. [PubMed: 12150886]
2. Coppieters KT, et al. Demonstration of islet-autoreactive CD8 T cells in insulitic lesions from recent onset and long-term type 1 diabetes patients. J Exp Med. 2012; 209:51–60. [PubMed: 22213807]
3. Culina S, et al. CD8(+) T cell frequencies in the pancreas, but not in blood, distinguish type 1 diabetic patients from healthy donors. Sci Immunol. 2018; 3
4. Schmidt RE, Murray C, Daley JF, Schlossman SF, Ritz J. A subset of natural killer cells in peripheral blood displays a mature T cell phenotype. J Exp Med. 1986; 1:351–356.
5. Zhou J, et al. High circulating CD3+CD56+CD16+ natural killer-like T cell levels predict a better IVF treatment outcome. J Reprod Immunol. 2013; 97:197–203. [PubMed: 23452704]
6. Diao H, et al. A possible role for NKT-like cells in patients with chronic hepatitis B during telbivudine treatment. Immunol Lett. 2014; 160:65–71. [PubMed: 24718278]
7. Galgani M, et al. Meta-immunological profiling of children with type 1 diabetes identifies new biomarkers to monitor disease progression. Diabetes. 2013; 62:2481–2491. [PubMed: 23396400]
8. Atkinson MA, et al. How does type 1 diabetes develop?: the notion of homicide or β-cell suicide revisited. Diabetes. 2011; 60:1370–1379. [PubMed: 21525508]
9. Beato-Víbora PI, Tormo-García MÁ. Glycemic control and insulin requirements in type 1 diabetic patients depending on the clinical characteristics at diabetes onset. Endocr Res. 2014; 39:86–90. [PubMed: 24152206]
10. Pipkin ME, et al. Interleukin-2 and inflammation induce distinct transcriptional programs that promote the differentiation of effector cytolytic T cells. Immunity. 2010; 32:79–90. [PubMed: 20096607]
11. Kalia V, et al. Prolonged interleukin-2Ralpha expression on virus-specific CD8+ T cells favors terminal-effector differentiation in vivo. Immunity. 2010; 32:91–103. [PubMed: 20096608]
12. Alter G, Malenfant JM, Altfeld M. CD107a as a functional marker for the identification of natural killer cell activity. J Immunol Methods. 2004; 294:15–22. [PubMed: 15604012]
13. Wagner JA, et al. CD56bright NK cells exhibit potent antitumor responses following IL-15 priming. J Clin Invest. 2017; 127:4042–4058. [PubMed: 28972539]
14. Yi JS, Holbrook BC, Michalek RD, Laniewski NG, Grayson JM. Electron transport complex I is required for CD8+ T cell function. J Immunol. 2006; 177:852–862. [PubMed: 16818739]
15. Bai A, et al. NADH oxidase-dependent CD39 expression by CD8(+) T cells modulates interferon gamma responses via generation of adenosine. Nat Commun. 2015; 9
16. Nazarewicz RR, Bikineyeva A, Dikalov SI. Rapid and specific measurements of superoxide using fluorescence spectroscopy. J Biomol Screen. 2013; 18:498–503. [PubMed: 23190737]

17. Criddle DN, et al. Menadione-induced reactive oxygen species generation via redox cycling promotes apoptosis of murine pancreatic acinar cells. J Biol Chem. 2006; 281:40485–40492. [PubMed: 17088248]
18. Terrazzano G, et al. T cell activation induces CuZn superoxide dismutase (SOD)-1 intracellular re-localization, production and secretion. Biochim Biophys Acta. 2014; 1843:265–274. [PubMed: 24184207]
19. Wicker LS, et al. Type 1 diabetes genes and pathways shared by humans and NOD mice. J Autoimmun. 2005; 25:29–33. [PubMed: 16257508]
20. Roep BO. The role of T-cells in the pathogenesis of Type 1 diabetes: from cause to cure. Diabetologia. 2003; 46:305–321. [PubMed: 12687328]
21. Dirice E, et al. Increased β-cell proliferation before immune cell invasion prevents progression of type 1 diabetes. Nat Metab. 2019; 1:509–518. [PubMed: 31423480]
22. Pugliese A. Autoreactive T cells in type 1 diabetes. J Clin Invest. 2017; 127:2881–2891. [PubMed: 28762987]
23. Pinkse GG, et al. Autoreactive CD8 T cells associated with beta cell destruction in type 1 diabetes. Proc Natl Acad Sci USA. 2005; 102:18425–1830. [PubMed: 16339897]
24. Sivori S, et al. Human NK cells: surface receptors, inhibitory checkpoints, and translational applications. Cell Mol Immunol. 2019; 16:430–441. [PubMed: 30778167]
25. Tan TG, Mathis D, Benoist C. Singular role for T-BET+CXCR3+ regulatory T cells in protection from autoimmune diabetes. Proc Natl Acad Sci USA. 2016; 113:14103–14108. [PubMed: 27872297]
26. van Halteren AG, Kardol MJ, Mulder A, Roep BO. Homing of human autoreactive T cells into pancreatic tissue of NOD-scid mice. Diabetologia. 2005; 48:75–82. [PubMed: 15619074]
27. Shan Z, Xu B, Mikulowska-Mennis A, Michie SA. CCR7 directs the recruitment of T cells into inflamed pancreatic islets of nonobese diabetic (NOD) mice. Immunol Res. 2014; 58:351–357. [PubMed: 24687731]
28. Rudensky AY. Regulatory T cells and Foxp3. Immunol Rev. 2011; 241:260–268. [PubMed: 21488902]
29. Godfrey DI, Kronenberg M. Going both ways: immune regulation via CD1d-dependent NKT cells. J Clin Invest. 2004; 114:1379–1388. [PubMed: 15545985]
30. Kuylenstierna C, et al. NKG2D performs two functions in invariant NKT cells: direct TCR-independent activation of NK-like cytolysis and co-stimulation of activation by CD1d. Eur J Immunol. 2011; 41:1913–1923. [PubMed: 21590763]
31. Wirasinha RC, et al. GPR65 inhibits experimental autoimmune encephalomyelitis through CD4(+) T cell independent mechanisms that include effects on iNKT cells. Immunol Cell Biol. 2018; 96:128–136. [PubMed: 29363187]
32. Lin YL, Lin SC. Analysis of the CD161-expressing cell quantities and CD161 expression levels in peripheral blood natural killer and T cells of systemic lupus erythematosus patients. Clin Exp Med. 2017; 17:101–109. [PubMed: 26590595]
33. Mingari MC, Pietra G, Moretta L. Immune Checkpoint Inhibitors: Anti-NKG2A Antibodies on Board. Trends Immunol. 2019; 40:83–85. [PubMed: 30609967]
34. De Simone M, et al. Transcriptional Landscape of Human Tissue Lymphocytes Unveils Uniqueness of Tumor-Infiltrating T Regulatory Cells. Immunity. 2016; 45:1135–1147. [PubMed: 27851914]
35. Schmidleithner L, et al. Enzymatic Activity of HPGD in Treg Cells Suppresses Tconv Cells to Maintain Adipose Tissue Homeostasis and Prevent Metabolic Dysfunction. Immunity. 2019; 50:1232–1248.e14. [PubMed: 31027998]
36. Craig ME, Hattersley A, Donaghue KC. Definition, epidemiology and classification of diabetes in children and adolescents. Pediatr Diabetes. 2009; 12:3–12.
37. Report of Working Group of European Society of Paediatric Gastroenterology and Nutrition. Revised criteria for diagnosis of coeliac disease. Arch Dis Child. 1990; 65:909–911. [PubMed: 2205160]
38. Hanley P, Lord K, Bauer AJ. Thyroid Disorders in Children and Adolescents: A Review. JAMA Pediatr. 2016; 170:1008–1019. [PubMed: 27571216]

39. Bruzzaniti S, et al. An immunometabolic pathomechanism for chronic obstructive pulmonary disease. Proc Natl Acad Sci USA. 2019; 116:15625–15634. [PubMed: 31308239]
40. McGinnes K, Chapman G, Marks R, Penny R. A fluorescence NK assay using flow cytometry. J Immunol Methods. 1986; 86:7–15. [PubMed: 3944470]
41. Tallerico R, et al. Human NK cells selective targeting of colon cancer-initiating cells: a role for natural cytotoxicity receptors and MHC class I molecules. J Immunol. 2013; 190:2381–2390. [PubMed: 23345327]
42. Terrazzano G, et al. Differential involvement of CD40, CD80, and major histocompatibility complex class I molecules in cytotoxicity induction and interferon-gamma production by human natural killer effectors. J Leukoc Biol. 2002; 72:305–311. [PubMed: 12149421]
43. Sabbatini M, et al. Oscillatory mTOR inhibition and Treg increase in kidney transplantation. Clin Exp Immunol. 2015; 182:230–240. [PubMed: 26077103]
44. Del Fabbro C, Scalabrin S, Morgante M, Giorgi FM. An extensive evaluation of read trimming effects on Illumina NGS data analysis. PLoS One. 2013; 8:e85024. [PubMed: 24376861]
45. Martin M. Cutadapt removes adapter sequences from high-throughput sequencing reads. EMBnet journal. 2011; 17:10–12.
46. Dobin A, et al. STAR: ultrafast universal RNA-seq aligner. Bioinformatics. 2013; 29:15–21. [PubMed: 23104886]
47. Pertea M, et al. StringTie enables improved reconstruction of a transcriptome from RNA-seq reads. Nat Biotechnol. 2015; 33:290–295. [PubMed: 25690850]
48. Anders S, Pyl PT, Huber W. HTSeq--a Python framework to work with high-throughput sequencing data. Bioinformatics. 2015; 31:166–169. [PubMed: 25260700]
49. Love MI, Huber W, Anders S. Moderated estimation of fold change and dispersion for RNA-seq data with DESeq2. Genome Biol. 2014; 15:550. [PubMed: 25516281]

Anders S, Huber W. Differential expression analysis for sequence count data. Genome Biol. 2010; 11:R106. [PubMed: 20979621]

Europe PMC Funders Author Manuscripts

Europe PMC Funders Author Manuscripts

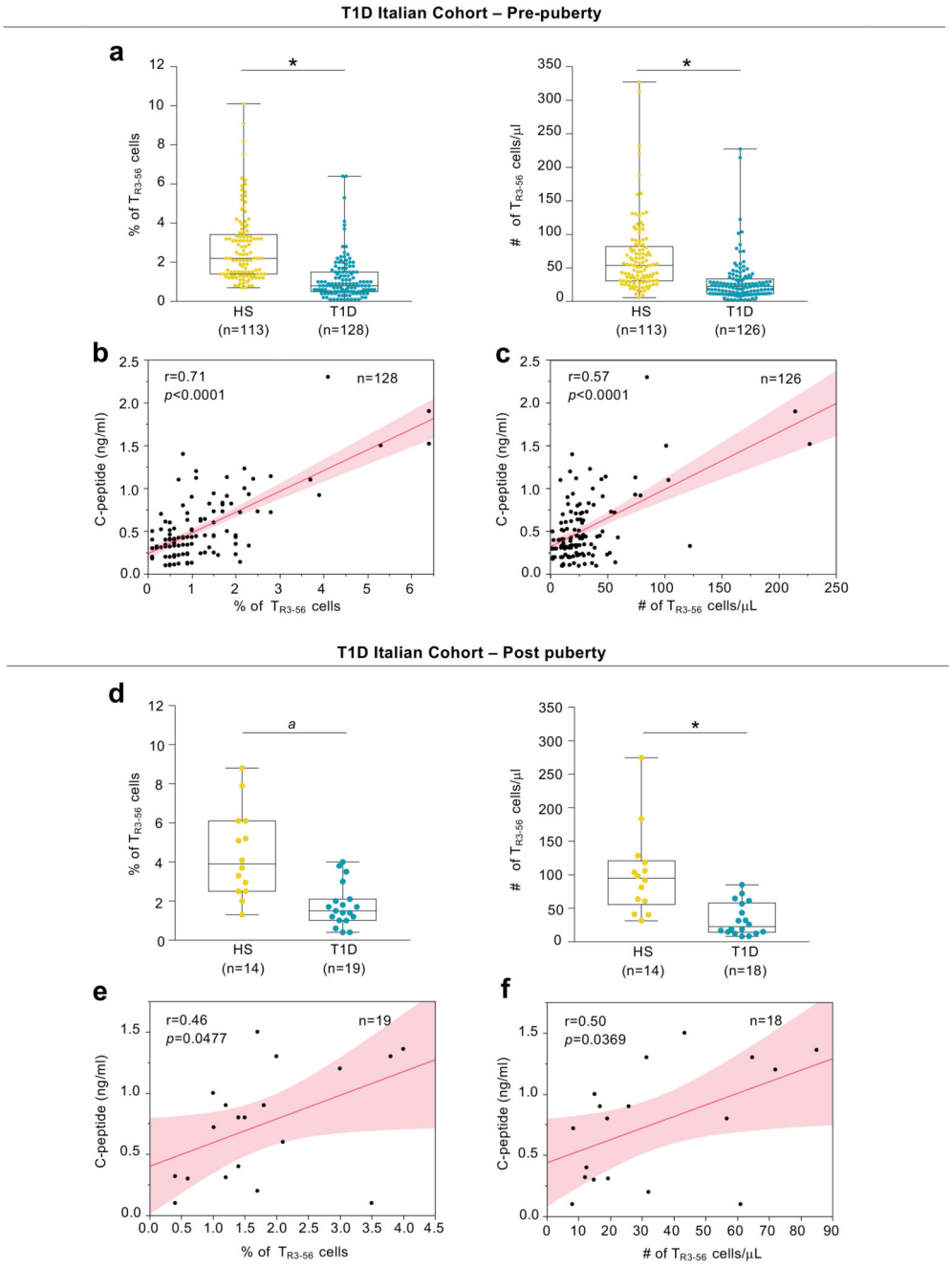

Fig. 1. $T_{R3\text{-}56}$ cell enumeration predicts residual β-cell function in T1D subjects at disease onset.

a, Percentage (left) and absolute number (right) of circulating $T_{R3\text{-}56}$ cells in pre-puberty T1D subjects (n=128 for percentage and n=126 for absolute number, respectively) at disease onset (Italian cohort), as compared with age-, sex-related healthy subjects (n=113). Data are presented as box plots (min, max, median, and 25th and 75th percentiles), each dot represents a individual subject. *p<0.0001 by two-tailed Mann-Whitney U-test. **b**, Scatter plot showing positive correlation between the frequency of circulating $T_{R3\text{-}56}$ cells and serum levels of fasting C-peptide in pre-puberty subjects (Italian cohort) affected by T1D

Europe PMC Funders Author Manuscripts

(n=128) at disease onset; r=0.71, $p<0.0001$ by two-tailed Pearson's correlation. Red line indicates regression line and shading indicates confidence interval. **c**, Scatter plot showing positive correlation between the absolute number of circulating $T_{R3\text{-}56}$ cells and serum levels of fasting C-peptide in pre-puberty T1D subjects (n=126) at disease onset from Italian cohort; r=0.57, $p<0.0001$ by two-tailed Pearson's correlation. Red line indicates regression line and shading indicates confidence interval. **d**, Box plots indicate the percentage (left) and absolute number (right) of circulating $T_{R3\text{-}56}$ cells in post-puberty young adults T1D (n=19 for percentage and n=18 for absolute number, respectively) at disease onset (Italian cohort), as compared with age-sex related healthy subjects (n=14). Each dot represents an individual subject. Data are shown as described for **a**. $^{a}p=0.0001$, $^{*}p<0.0001$ by two-tailed Mann-Whitney U-test. **e**, Scatter plot showing positive correlation between the frequency of circulating $T_{R3\text{-}56}$ cells and serum levels of fasting C-peptide in post-puberty young adults T1D (n=19) at disease onset from Italian cohort; r=0.46, $p=0.0477$ by two-tailed Pearson's correlation. Red line indicates regression line and shading indicates confidence interval. **f**, Scatter plot showing the correlation between the absolute number of circulating $T_{R3\text{-}56}$ cells and serum levels of fasting C-peptide in post-puberty young adults T1D (n=18) from Italian cohort; r=0.50, $p=0.0369$ by two-tailed Pearson's correlation. Red line indicates regression line and shading indicates confidence interval.

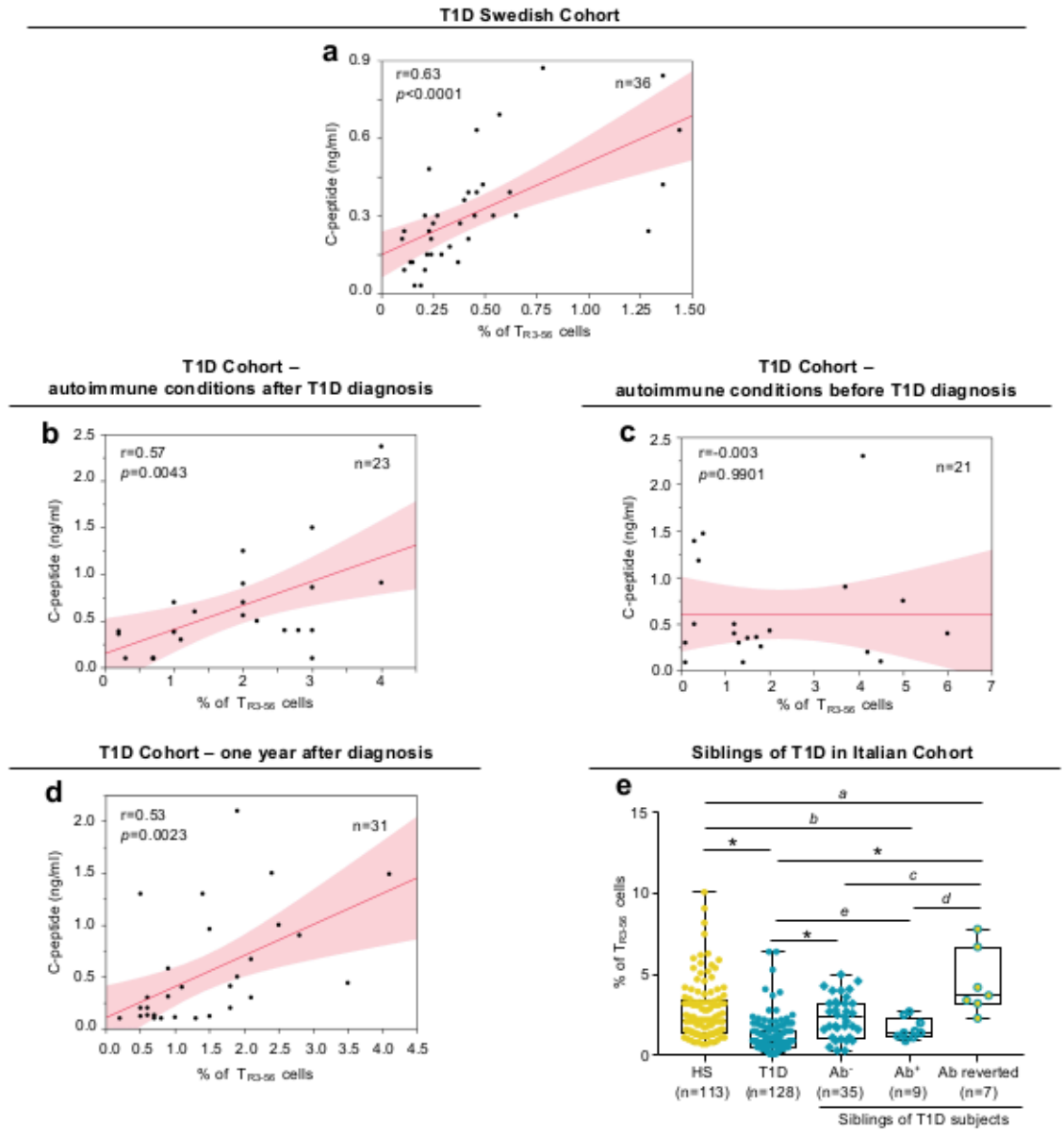

Fig. 2. Validation and specificity of $T_{R3\text{-}56}$ cell predictive role.

a, Scatter plot showing positive correlation between the frequency of circulating $T_{R3\text{-}56}$ cells and serum levels of fasting C-peptide in a validation cohort (Swedish cohort) of T1D children (n=36) at disease onset; r=0.63, p<0.0001 by two-tailed Pearson's correlation. Red line indicates regression line and shading indicates confidence interval. **b**, Scatter plot showing positive correlation between the frequency of circulating $T_{R3\text{-}56}$ cells and serum levels of fasting C-peptide in a cohort of T1D children that developed other autoimmune conditions after T1D diagnosis (n=23); r=0.57, p=0.0043 by two-tailed Pearson's correlation. Red line indicates regression line and shading indicates confidence interval. **c,** Scatter plot showing the absence of statistical correlation between the frequency of circulating $T_{R3\text{-}56}$ cells and serum levels of fasting C-peptide in children (n=21) that at T1D diagnosis were

Europe PMC Funders Author Manuscripts

already affected by other autoimmune conditions (CD or AIT); r=-0.003, p=0.9901 by two-tailed Pearson's correlation. Red line indicates regression line and shading indicates confidence interval. **d,** Scatter plot showing positive correlation between the frequency of circulating $T_{R3\text{-}56}$ cells and serum levels of fasting C-peptide in T1D subjects one year after diagnosis (Italian cohort) (n=31); r=0.53, p=0.0023 by two-tailed Pearson's correlation. Red line indicates regression line and shading indicates confidence interval. **e,** Box plot indicates the frequency of $T_{R3\text{-}56}$ cells in healthy subjects (n=113), T1D children at diagnosis (n=128) and in 51 at-risk siblings of T1D individuals: 35 autoantibody negative (Ab^-), 9 autoantibody positive (Ab^+) and 7 autoantibody positive reverted to autoantibody negative (Ab reverted) subjects. Data are presented as box plots (min, max, median, and 25th and 75th percentiles), each dot represents a individual subjects. $^a p$=0.0084; $^b p$=0.0456; $^c p$=0.006; $^d p$=0.0007; $^e p$=0.0106; *p<0.0001 by two-tailed Mann-Whitney U-test.

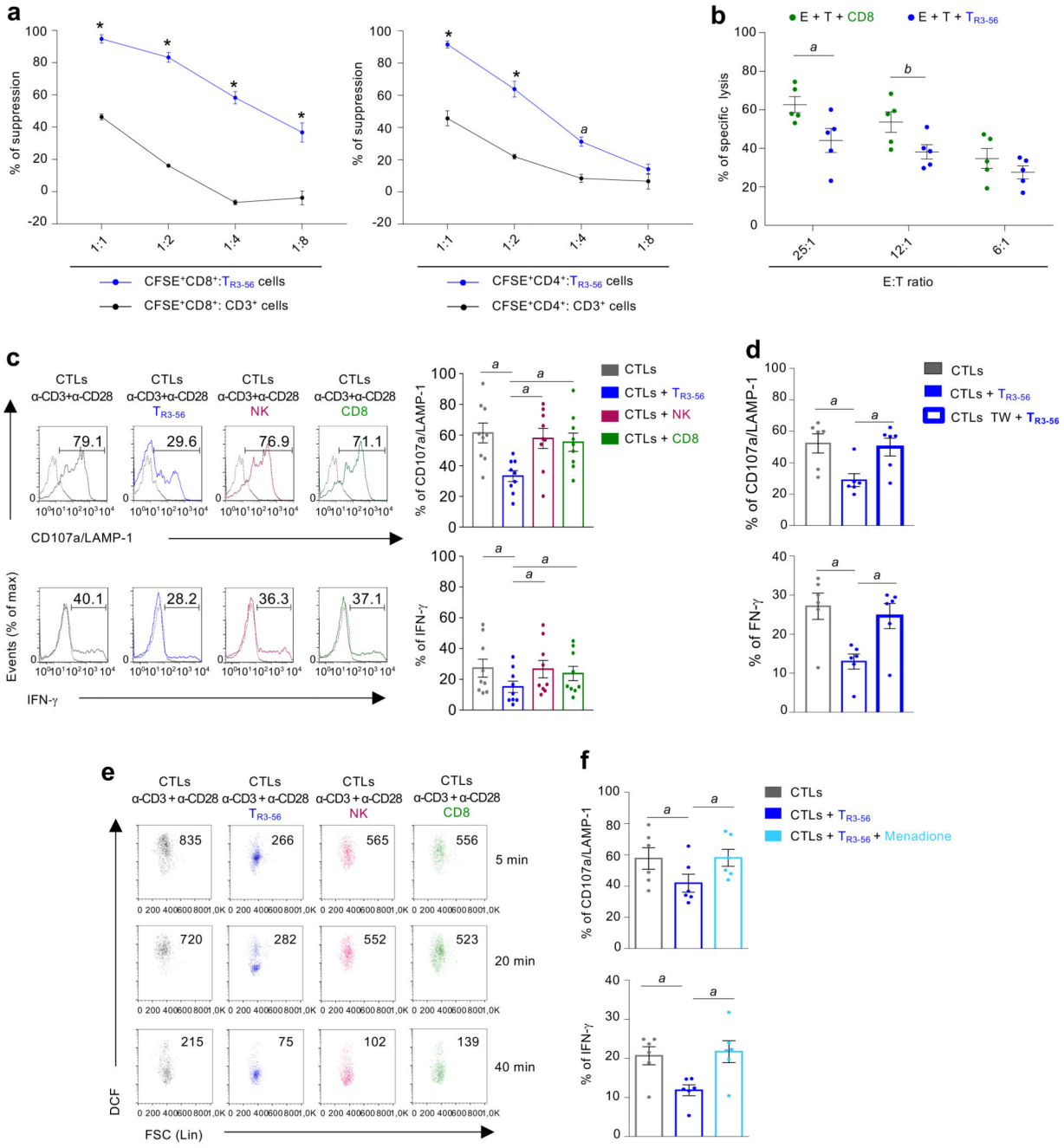

Fig. 3. T_{R3-56} cells regulate $CD8^+$ effector functions by modulating intracellular ROS levels.

a, Suppression exerted by T_{R3-56} (blue) or control cells on the proliferation of CFSE-labelled $CD8^+$ (left panel) and CFSE-labelled $CD4^+$ (right panel) lymphocytes TCR-stimulated for 72 hours *in vitro*, at different ratios. Data are from independent experiments, n=6 for T_{R3-56} cells and n=3 for $CD3^+$ cells. Error bars represent SEM. $^a p$=0.0013; ****p<0.0001 by two-way ANOVA corrected for multiple comparison using Bonferroni test. **b**, Cytolytic activity of CTLs against allogeneic PBMCs. PBMCs (target) are CFDA-labelled and co-cultured for 3 hours with allogenic CTLs, either in the presence of T_{R3-56} or

control cells (see also Supplementary Figure 3). Data are from five independent experiments (n=5). ^{a}p=0.0376; ^{b}p=0.0460 by two-tailed Student's *t*-test. Data are expressed as mean ± SEM. **c**, Left, CD107a/LAMP-1 and IFN-γ staining of CTLs after 4 hours stimulation *via* TCR alone (grey), in the presence of $T_{R3\text{-}56}$ (blue) or control cells (see also Supplementary Figure 4). Data are from one representative experiment out of nine. Dotted lines indicate unstimulated cells. Numbers indicate percentage of positive cells. Right, cumulative data from nine independent experiments. Data are expressed as mean ± SEM. ^{a}p=0.0039 by two-tailed Wilcoxon matched pairs test. **d**, CD107a/LAMP-1 and IFN-γ from CTLs stimulated for 4 hours *via* TCR alone (grey), in the presence of $T_{R3\text{-}56}$ cells (blue) or when $T_{R3\text{-}56}$ cells were separated in transwell plate (bold blue). Data are expressed as mean ± SEM. Data are from six independent experiments (n=6). ^{a}p=0.013 by two-tailed Wilcoxon matched pairs test. **e**, Kinetics of DCF staining, as a measure of intracellular ROS levels, of CTLs TCR-stimulated alone (grey) with $T_{R3\text{-}56}$ (blue), or in the presence of control cells. Numbers in plot show the MFI. Data are from one representative experiment out of three. **f**, CD107a/LAMP-1 and IFN-γ production by CTLs stimulated for 4 hours *via* TCR alone (grey) or in the presence of $T_{R3\text{-}56}$ cells (blue); light blue boxes indicate co-culture of $T_{R3\text{-}56}$ cells with menadione pre-treated CTLs. Data are from six independent experiments. Data are expressed as mean ± SEM. ^{a}p=0.013 by two-tailed Wilcoxon matched pairs test.

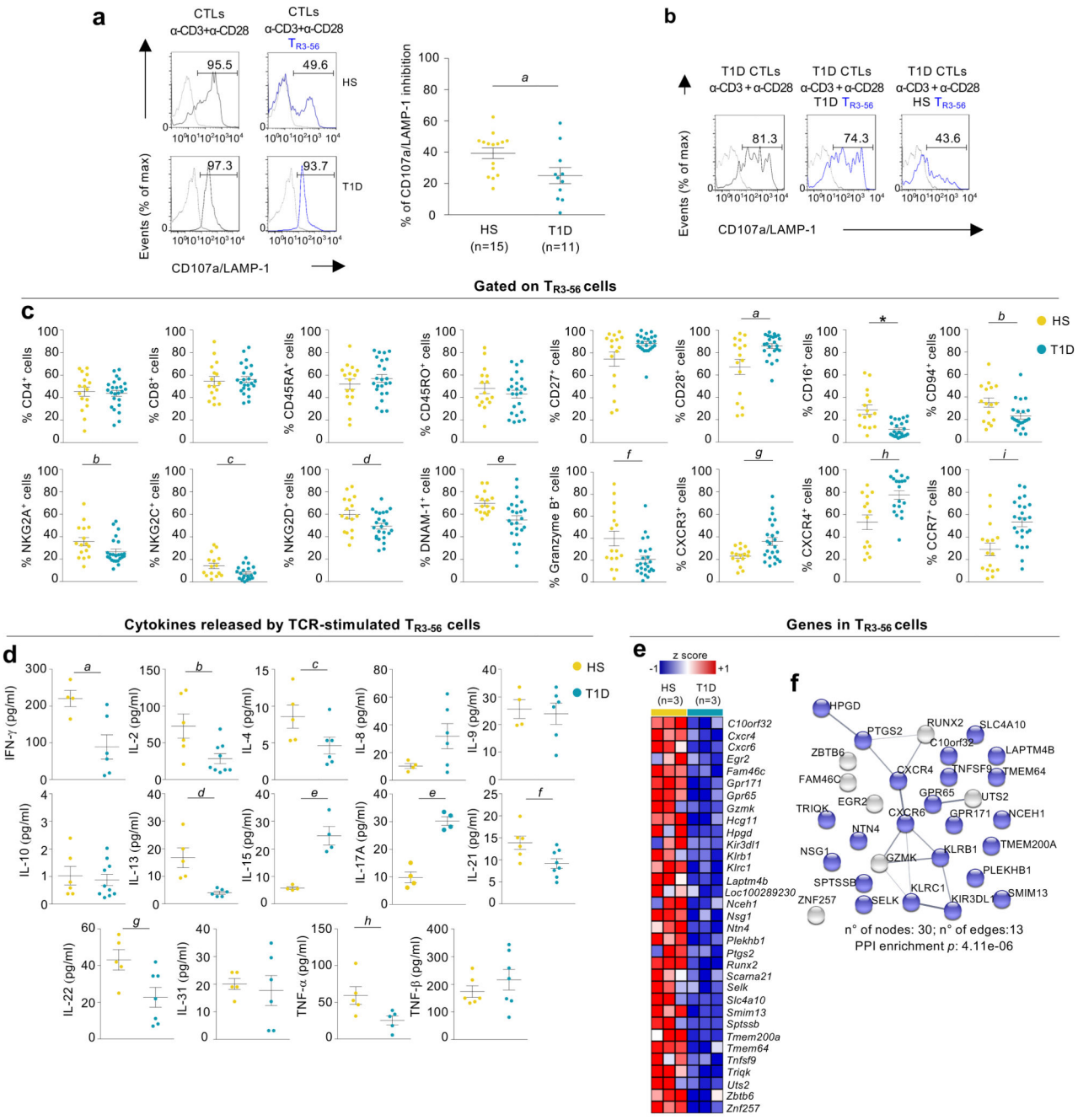

Fig. 4. Functional and molecular dysregulation of $T_{R3\text{-}56}$ cells from recent-onset T1D children.

a, CD107a/LAMP-1 staining of CTLs TCR-stimulated for 4 hours alone (grey) or with autologous $T_{R3\text{-}56}$ cells (blue) from one representative healthy (upper) and T1D individual (lower). Right, suppression of CD107a/LAMP-1 in CTLs from T1D (n=11) and healthy subjects (n=15), in presence of autologous $T_{R3\text{-}56}$ cells. Each dot represents an individual subject. Data are expressed as mean ± SEM. [a]p=0.0456 by two-tailed Mann-Whitney U-test. **b**, CD107a/LAMP-1 expression in CTLs, from T1D subject, TCR-stimulated for 4 hours alone (left), in the presence of autologous (middle) or allogeneic (right) $T_{R3\text{-}56}$ cells from a

Europe PMC Funders Author Manuscripts

control. Data are from one representative experiment out of three. Dotted lines indicate unstimulated CTLs. Numbers indicate percentage of positive cells. **c**, Expression of molecules on $T_{R3\text{-}56}$ cells from healthy and T1D individuals. Data are from n=16 HS, n=24 T1D for all molecules except for CD94 (n=16 HS, n=22 T1D), NKG2C (n=16 HS, n=21 T1D) and CXCR4 (n=14 HS, n=19 T1D). Each dot represents an individual subject. Data are expressed as mean ± SEM. ^{a}p=0.04; ^{b}p=0.0442; ^{c}p=0.0294; ^{d}p=0.044; ^{e}p=0.0062; ^{f}p=0.0147; ^{g}p=0.0211; ^{h}p=0.0041; ^{i}p=0.0010; *p<0.0001 by two-tailed Mann-Whitney U-test. **d**, Cytokines released by $T_{R3\text{-}56}$ cells TCR-activated for 48 hours *in vitro* from healthy and T1D individuals (n=4 HS, n=6 T1D for IFN-γ, IL-8 and IL-9; n=5 HS, n=6 T1D for IL-4, IL-13 and IL-31; n=4 HS and T1D for IL-15 and IL-17A; n=6 HS, n=9 T1D for IL-2; n=6 HS, n=10 T1D for IL-10; n=6 HS, n=8 T1D for IL-23; n=5 HS, n=7 T1D for IL-22; n=5 and T1D for TNF-α; n=6 HS, n=7 T1D for TNF-β). Each dot represents an individual subject. Data are expressed as mean ± SEM. ^{a}p=0.0381; ^{b}p=0.0132; ^{c}p=0.0476; ^{d}p=0.0043; ^{e}p=0.0286; ^{f}p=0.0426; ^{g}p=0.0366; ^{h}p=0.0317 by two-tailed Mann-Whitney U-test. **e**, Heatmap of z-scored RNA-Seq expression values of 33 genes with a $\log_2$FoldChange<-1.0 in comparison of $T_{R3\text{-}56}$ cells from healthy and T1D subjects (n=3 for group). **f**, Protein-protein interaction network reconstructed from STRING database and differentially expressed transcripts ($\log_2$FoldChange<-1.0 as in e) identified by comparing RNA-Seq profiles from $T_{R3\text{-}56}$ cells of both group (n=3 for group) by non-parametric/permutation-based and multiple testing correction according to Benjamini and Hochber. In blue, 23 genes leading to a significant enrichment of the cellular component “membrane” (GO:0016020) (FDR=0.0059).

Europe PMC Funders Author Manuscripts